Fig. 1. Examination using TOCU. The probe tip is inserted transorally and gently touched to the pharyngeal posterolateral wall in a healthy volunteer.

Methods

Three cases with carotid stenosis are described in which CEA was presumed to be preferable, but the ICA lesion could hardly be estimated by conventional carotid ultrasonography. In these cases, TOCU was performed in addition to conventional carotid ultrasonography with insonation from the surface of the neck and cerebral angiography. The Hitachi-ATL HDI 5000 was used for the TOCU with the 9- to 5-MHz convex array transducer, a commercially available probe for rectal ultrasonography. The 12- to 5-MHz linear array transducer was used for conventional carotid ultrasonography with the Hitachi-ATL HDI 5000. The methods for TOCU have been described previously [7]. Briefly, the tip of the probe covered with a clean rubber cover was placed at the posterior pharyngeal wall of the patient in a supine position (fig. 1). The ICA, external carotid artery, and jugular vein could be identified. The extracranial distal ICA could be visualized as a vertical linear line bent slightly backward. The properties of the blood vessel were evaluated by the B-mode as well as by color flow imaging. Doppler blood flow measurements were also made. The examination could be performed within 20 min without any local anesthesia, since the pharyngeal stimulation could be endured in the present cases.

Case Reports

Case 1

A 73-year-old man was admitted to our hospital with a repetitive transient weakness of the left upper and lower limbs. On admission, clinical examination revealed right carotid bruit but no neurological abnormalities. Cerebral angiography showed 93% stenosis at the origin of the right ICA which was estimated by the North American Symptomatic Carotid Endarterectomy Trial method [1] (fig. 2A). Conventional carotid ultrasound revealed an increased end-diastolic flow ratio of the common carotid artery of 2.56 (left 2.87 cm/s, right 11.2 cm/s), suggesting a significant occlusive lesion at the right ICA. However, the distal end of the right ICA stenosis ranged beyond the mandibular bone and the poststenotic lesion of the right ICA could not be observed by conventional carotid ultrasound. It was planned that he would undergo CEA. However, just before the operation, occlusion of the right ICA was highly suspected because of the loss of the carotid bruit that had been heard up until then. Since the poststenotic blood flow in the right ICA could not be detected by conventional carotid ultrasonography (fig. 2B), TOCU was performed instead. TOCU (fig. 2C) clearly showed the presence of distal blood flow of the right ICA, indicating high-grade stenosis rather than occlusion and CEA was then performed.

Case 2

A 63-year-old woman was transferred to our hospital because of a weakness in the left upper and lower limbs. Clinical examination showed left hemiparesis and MRI revealed an infarction in the right frontal lobe in the territory of middle cerebral artery. Cerebral angiography revealed that 71% stenosis was present at the origin of the left ICA and that the carotid bifurcation was situated at a high position above the mandibular angle (fig. 3A). Carotid ultrasonography showed that the end-diastolic flow ratio of the common carotid artery reached 3.25 (left 22.7 cm/s, right 6.97 cm/s), indicating the presence of a significant lesion at the right ICA. Conventional carotid ultrasonography could not detect the right ICA lesion since the proper insonation was prevented due to not only high location of carotid bifurcation but also severe calcification with an acoustic shadow (fig. 3B). CEA was considered to be beneficial for her in the prevention of further ischemic stroke. Prior to the surgery, TOCU was performed again and demonstrated unexpectedly that blood flow at the poststenotic region of the left ICA disappeared, indicating the occlusion of the artery (fig. 3C). Thereafter, right ICA occlusion was also confirmed by cerebral angiography (fig. 3D) and CEA was abandoned.

Case 3

A 69-year-old man was admitted to our hospital due to transient monocular blindness in his left eye. Cerebral angiography revealed that the origin of the left ICA was severely stenosed and the poststenotic part of the extracranial ICA appeared to be narrowed till the intracranial portion (fig. 4A). Although the conventional carotid ultrasound showed a high end-diastolic flow ratio of the common carotid artery of 2.07 (right 33.1 cm/s, left 16.0 cm/s), the peripheral blood flow distal to the stenosis could not be observed because of the high position of carotid bifurcation (fig. 4C). Then, the TOCU was performed and revealed a reduced diameter without any organic lesion, and the presence of anterograde blood flow in the poststenotic part of the left ICA, suggesting a collapse of the artery [7, 8] (fig. 4B). After CEA, the left ICA diameter dilated from 2.7 to 4.5 mm and the blood flow in the distal portion of the ICA increased remarkably (fig. 4D–F).

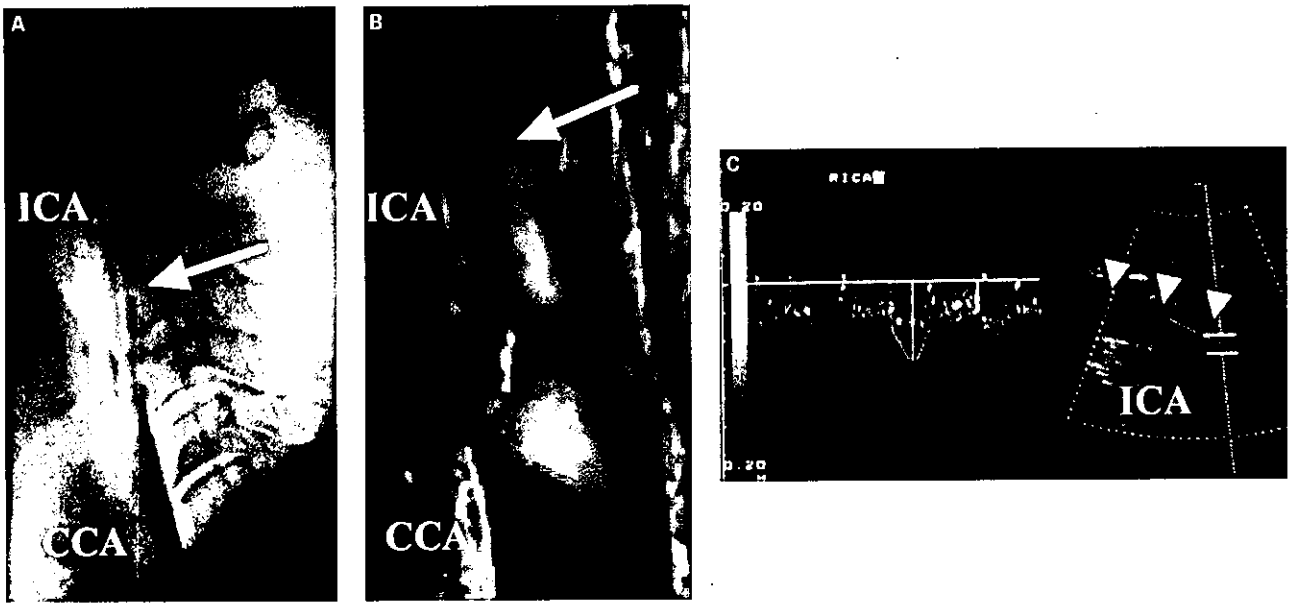

Fig. 2. Case 1. **A** Carotid angiogram revealed a stenosis in the origin of the ICA (arrow). **B** Color flow image observed using conventional carotid ultrasonography. Blood flow could not be detected in the distal portion of the ICA. The arrow indicates the identical portion of the carotid stenosis shown in **A**. **C** Duplex scan image of the distal portion of the ICA obtained by TOCU. Doppler flow velocity (right panel) and B-mode imaging clearly show the patency of the distal portion of the ICA (arrow head).

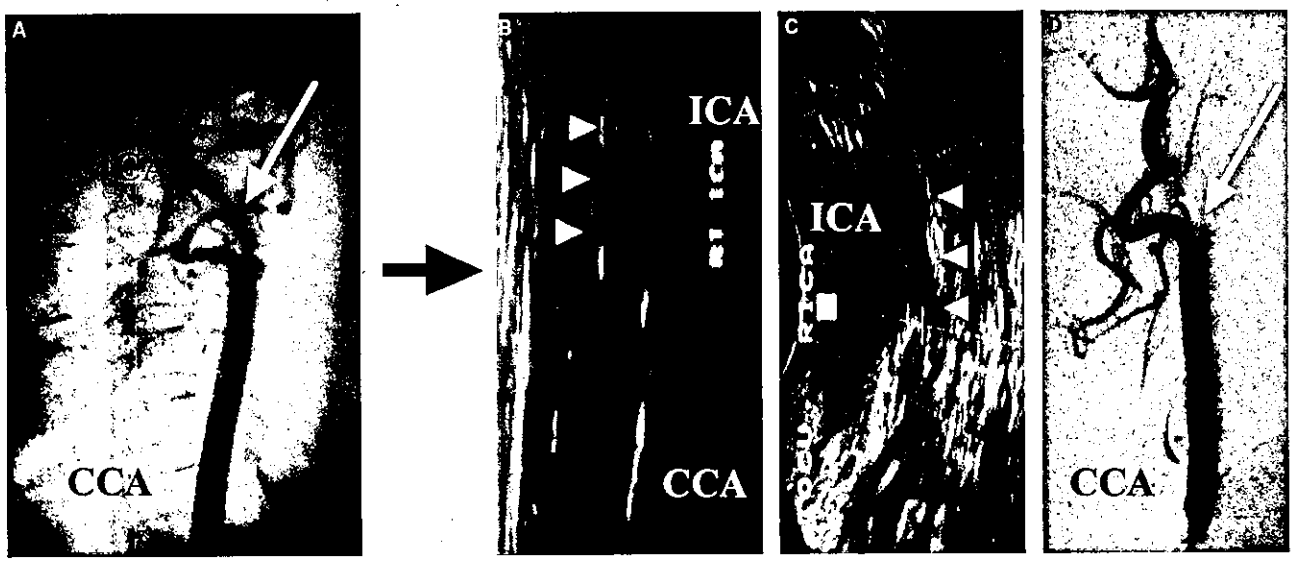

Fig. 3. Case 2. **A** High-grade stenosis in the origin of the ICA could be seen in the carotid angiogram (arrow). **B** B-mode imaging observed using conventional carotid ultrasonography. Note that the carotid plaque is heavily calcified, thus preventing adequate insonation (arrow heads). **C** Color flow image in the distal ICA obtained by TOCU. No blood flow could be detected in the distal ICA (arrow heads). **D** Carotid angiogram revealing the occlusion of the ICA in the origin.

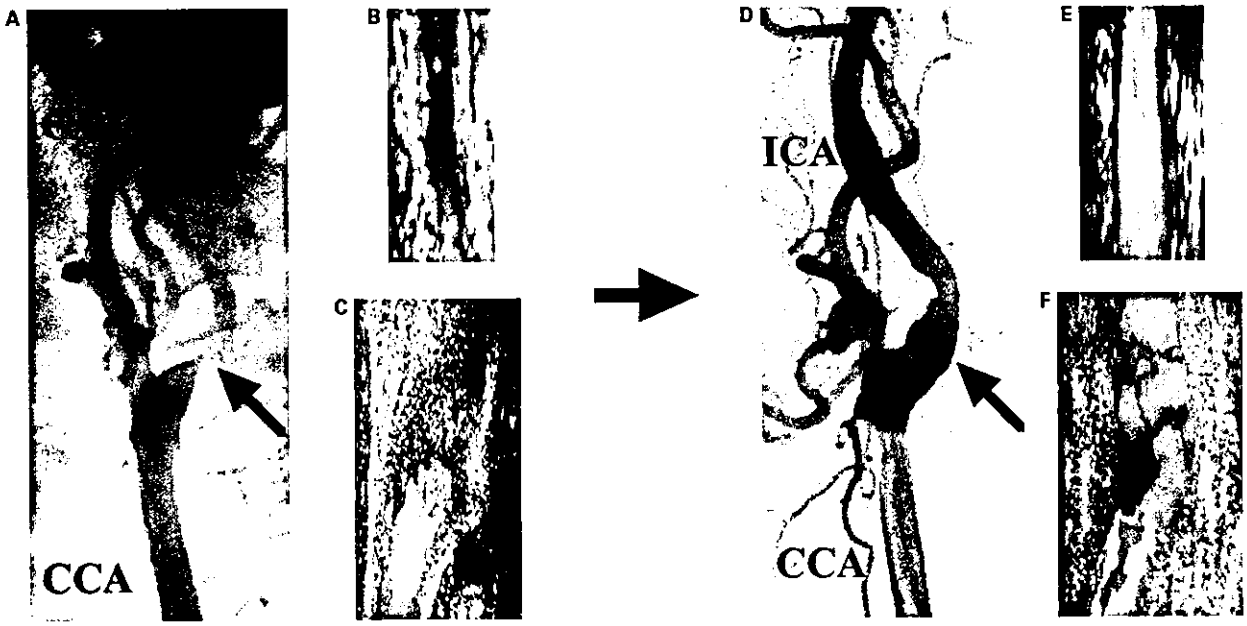

Fig. 4. Case 3. The angiographic and ultrasonographic findings in the carotid arteries before (left panels) and after CEA (right panels). The arrow indicate severe stenosis in the origin of the ICA (**A**). Angiographic (**A, D**), transoral carotid ultrasonographic (**B, E**) and conventional carotid ultrasonographic findings (**C, F**) are shown. After CEA, the collapsed distal ICA dilated remarkably.

Discussion

When CEA is considered to be beneficial for the patients with carotid stenosis, information concerning the pathological condition of the distal portion of the artery would be required in addition to the degree of the stenosis prior to the surgery. Cerebral angiography is the standard tool for the assessment and has been performed so far. However, it is incapable of evaluating the properties of the blood vessel wall and the vessel diameter. Moreover, it is an invasive procedure with possible complications and for practical reasons cannot be performed repeatedly. Thus, noninvasive and easily repeatable techniques are desirable during the perioperative period of CEA.

Ultrasonography appears to be a useful tool since it can be performed noninvasively at the bedside. However, the conventional approach from the surface of the neck results in a restricted observational range under the mandibular bone and cannot be used to observe the distal portion of the ICA. Therefore, conventional carotid ultrasonography is useless when the carotid lesion is heavily calcified and/or carotid bifurcation is located at a higher position. It has been reported quite recently that distal ICA could be visualized with a 3.5-MHz convex probe [9]. However, the observation range is still limited by the conventional approach. Moreover, in the case of tight carotid stenosis, it is often difficult to differentiate between occlusion and high-grade stenosis close to the occlusion using conventional carotid ultrasonography. Because of these limitations, we have explored whether TOCU can provide the additional information required in CEA patients. Throughout our experiences, 3 cases with high carotid bifurcation, severe calcified plaque and near-occlusion were found to have had benefited from TOCU investigation which critically affected the indication of CEA.

In cases 1 and 2 with carotid stenosis, conventional carotid ultrasonography from the surface of the neck could hardly provide sufficient information concerning the peripheral patency. On the other hand, TOCU clearly showed whether there was an occlusion or not. Besides, there is still the possibility that tight carotid stenosis may change to complete occlusion before CEA, as observed in case 2. In this case, TOCU is also useful for convenient differentiation.

In case 3, cerebral angiography depicted a narrowing of the ICA over the long segment. The following 4 situations would be possible: (1) although stenosis was restricted to the origin of the ICA, the peripheral vessel was collapsed

due to reduced flow caused by high-grade stenosis [7, 8], (2) the blood vessel lumen was narrowed over the long segment by an organic lesion, (3) the blood vessel diameter was narrowed over the long segment due to hypoplasia, and (4) the blood vessel was not filled with contrast medium, leading to laminar flow [10]. Angiography cannot differentiate these 4 states, but TOCU can. Although it is still difficult to differentiate between 1 and 3 by ultrasonography in the B-mode alone, they can be differentiated from each other by observing the presence of restricted proximal lesions and reduced Doppler flow velocity in the poststenotic lesion. Laminar flow may also be differentiated by discrepancy of the vessel diameter measured by TOCU and angiography [7]. In fact, case 3 was diagnosed as 1 according to TOCU findings and underwent CEA. After the operation, the collapsed peripheral blood vessel considerably dilated from 2.7 to 4.5 mm and the correctness of the diagnosis became evident.

TOCU is able to provide useful information about the characteristics of the distal ICA which can be obtained neither by conventional carotid ultrasonography nor by angiography. TOCU is a noninvasive and useful tool for convenient diagnosis of carotid stenosis in the perioperative period of CEA.

Acknowledgments

The authors thank Drs. Yasumori, Uda and Hitotsumatsu for their useful suggestions. This study was supported by Research Grants for Cardiovascular Diseases (14A-3) from the Ministry of Health and Welfare of Japan.

References

1 North American Symptomatic Carotid Endarterectomy Trial Collaborators: Beneficial effect of carotid endarterectomy in symptomatic patients with high-grade carotid stenosis. N Engl J Med 1991;325:445–453.

2 European Carotid Surgery Trialists' Collaborative Group: MRC European Carotid Surgery Trial: Interim results for symptomatic patients with severe (70–99%) or with mild (0–29%) carotid stenosis. Lancet 1991;337:1235–1243.

3 Mayberg MR, Wilson SE, Yatsu F, Weiss DG, Messina L, Hershey LA, Colling C, Eskridge J, Deykin D, Winn HR, for the Veterans Affairs Cooperative Studies Program 309 Trialist Group: Carotid endarterectomy and prevention of cerebral ischemia in symptomatic carotid stenosis. JAMA 1991;266:3289–3294.

4 Executive Committee for the Asymptomatic Carotid Atherosclerosis Study: Endarterectomy for asymptomatic carotid artery stenosis. JAMA 1995;273:1421–1428.

5 Handa N, Matsumoto M, Maeda H, Hougaku H, Kamada T, for the OSAKA Study Group: Ischemic stroke events and carotid atherosclerosis: Results of the Osaka follow-up study for ultrasonographic assessment of carotid atherosclerosis (the OSACA study). Stroke 1995;26:1781–1786.

6 Yasaka M, Kimura K, Otsubo R, Isa K, Wada K, Nagatsuka K, Minematsu K, Yamaguchi T: Transoral carotid ultrasonography. Stroke 1998;29:1383–1388.

7 Kishikawa K, Kamouchi M, Okada Y, Inoue T, Ibayashi S, Iida M: Evaluation of distal extracranial internal carotid artery by transoral carotid ultrasonography in patients with severe carotid stenosis. AJNR Am J Neuroradiol 2002;23:924–928.

8 Rothwell PM, Warlow CP: Low risk of ischemic stroke in patients with reduced internal carotid artery lumen diameter distal to severe symptomatic carotid stenosis. Stroke 2000;31:622–630.

9 Todo K, Watanabe M, Fukunaga R, Araki K, Yamamoto S, Rai M, Hoshi T, Nukata M, Taguchi A, Kinoshita N: Imaging of distal internal carotid artery by ultrasonography with a 3.5-MHz convex probe. Stroke 2002;33:1792–1794.

10 Kern MJ, Gibson P, Vandormael M: Alteration of 'jetlike' laminar flow after percutaneous transluminal angioplasty of saphenous vein bypass graft stenosis. Cathet Cardiovasc Diagn 1986;12:165–168.

Nox4 as the Major Catalytic Component of an Endothelial NAD(P)H Oxidase

Tetsuro Ago, MD; Takanari Kitazono, MD; Hiroaki Ooboshi, MD; Teruaki Iyama, MS; Youn Hee Han, PhD; Junichi Takada, MD; Masanori Wakisaka, MD; Setsuro Ibayashi, MD; Hideo Utsumi, PhD; Mitsuo Iida, MD

Background—Recent evidence has suggested that reactive oxygen species are important signaling molecules in vascular cells and play a pivotal role in the development of vascular diseases. The activity of NAD(P)H oxidase has been identified as the major source of reactive oxygen species in vascular endothelial cells. However, the precise molecular structure and the mechanism of activation of the oxidase have remained poorly understood.

Methods and Results—Here, we investigated the molecular identities and the superoxide-producing activity of endothelial NAD(P)H oxidase. We found that Nox4, a homologue of gp91phox/Nox2, was abundantly expressed in endothelial cells. The expression of Nox4 in endothelial cells markedly exceeded that of other Nox proteins, including gp91phox/Nox2, and was affected by cell growth. Using electron spin resonance and chemiluminescence, we measured the superoxide production and found that the endothelial membranes had an NAD(P)H-dependent superoxide-producing activity comparable to that of the neutrophil membranes, whereas the activity was not enhanced by the 2 recombinant proteins p47phox and p67phox, in contrast to that of the neutrophil membranes. Downregulation of Nox4 by an antisense oligonucleotide reduced superoxide production in endothelial cells in vivo and in vitro.

Conclusions—These findings suggest that Nox4 may function as the major catalytic component of an endothelial NAD(P)H oxidase. (***Circulation.*** **2004;109:227-233.)**

Key Words: reactive oxygen species ■ NAD(P)H oxidase ■ endothelium

Vascular endothelial cells seem to play an important role in regulation of vascular tone[1,2] and growth of vascular muscle cells.[3] During several disease states, such as hypertension, diabetes, and hypercholesterolemia, endothelial function seems to be deteriorated.[3] Such endothelial dysfunction may play a major role in the development of arteriosclerosis and cardiovascular disease. Reactive oxygen species (ROS), including hydrogen peroxide and superoxide, seem to be important signaling molecules in vascular cells.[4,5] It has been shown that the activity of NAD(P)H oxidase, a superoxide-producing enzyme, is present in vascular endothelial,[6] smooth muscle,[7] and adventitial cells[8] and contributes to the regulation of vascular tone[9] and to cardinal steps of the development of arteriosclerosis, ie, endothelial dysfunction,[3] abnormal smooth muscle cell growth,[10,11] and inflammation.[4]

The phagocyte NADPH oxidase is composed of 2 essential membrane-bound components, gp91phox/Nox2 and p22phox, which compose flavocytochrome b_{558}, and 4 cytosolic components, p47phox, p67phox, p40phox, and the small G protein Rac1/2.[12,13] Upon stimulation, the 4 cytosolic proteins translocate to the membrane, assemble with the cytochrome b_{558}, and thereby increase the activity of NADPH oxidase.[12–15] The activated oxidase produces a large amount of superoxide and plays a pivotal role in host defense against microbial infection.[12,13]

Conversely, the precise structure and the mechanisms of activation of the NAD(P)H oxidase in vascular endothelial cells are still poorly understood.[4,5] Although previous studies have confirmed that all of the oxidase components identical to the phagocyte NADPH oxidase are present in endothelial cells,[16–18] the endothelial NAD(P)H oxidase is considered to be different from the phagocyte oxidase in that the endothelial oxidase is continuously active at a low level even in the unstimulated conditions and the oxidase does not generate as high levels of ROS as the burst activity of the phagocytic enzyme.[9,16] Li and Shah[18] recently showed that the endothelial oxidase, in contrast to the phagocyte oxidase, exists as a preassembled intracellular complex associated with the cytoskeleton. Recently, 4 homologues of gp91phox/Nox2, called Nox1[10] and Nox3 to 5,[19–22] have been identified in nonphagocytic cells, and the simultaneous presence of multiple Nox proteins was demonstrated in one cell type,[23] raising the possibility that endothelial cells may also express another Nox protein.

Received February 20, 2002; de novo received August 8, 2003; revision received September 4, 2003; accepted September 8, 2003.

From the Department of Medicine and Clinical Science, Graduate School of Medical Sciences (T.A., T.K., H.O., J.T., M.W., S.I, M.I.), and Department of Biophysics, Graduate School of Pharmaceutical Sciences (T.I., Y.H.H., H.U.), Kyushu University, Fukuoka, Japan.

Correspondence to Tetsuro Ago, MD, PhD, Department of Medicine and Clinical Science, Graduate School of Medical Sciences, Kyushu University, Maidashi 3-1-1, Higashi-ku, Fukuoka 812-8582, Japan. E-mail agou@intmed2.med.kyushu-u.ac.jp

Circulation is available at http://www.circulationaha.org

DOI: 10.1161/01.CIR.0000105680.92873.70

TABLE 1. Nucleotide Sequences of Primers Used for RT-PCR

	Forward (5′–3′)	Reverse (5′–3′)
r p22phox*	TGGCCTGATCCTCATCACAG	AGGCACGGACAGCAGTAAGT
h p22phox*	GTACTTTGGTGCCTACTCCA	CGGCCCGAACATAGTAATTC
r and h Nox1*	CTTCCTCACTGGCTGGGATA	TGACAGCATTTGCGCAGGCT
r and h gp91phox/Nox2*	CCAGTGAAGATGTGTTCAGCT	GCACAGCCAGTAGAAGTAGAT
r and h gp91phox/Nox2	ATGGGGAACTGGGCTGTGAAT	TTAGAAGTTTTCCTTGTTGAA
h gp91phox/Nox2	TGTCCAAGCTGGAGTGGCAC	GCACAGCCAGTAGAAGTAGAT
r and h Nox3	GAGTGGCACCCCTTCACCCT	CTAGAAGCTCTCCTTGTTGT
r and h Nox4*	AGTCAAACAGATGGGATA	TGTCCCATATGAGTTGTT
r and h Nox5	AAGCATACTTGCCCCAGCTG	CAGGCCAATGGCCTTCATGT
r p47phox*	TCACCGAGATCTACGAGTTC	TCCCATGAGGCTGTTGAAGT
h p47phox*	TTGAGAAGCGCTTCGTACCC	CGTCAAACCACTTGGGAGCT
r and h p67phox*	CAGTTCAAGCTGTTTGCCTG	TTCTTGGCCAGCTGAGCCAC
r and h GAPDH*	TGAACGGGAAGCTCACTGG	TCCACCACCCTGTTGCTGTA
r and h cyclophilin B*	ATGGCACAGGAGGAAAGAGC	ATGATCACATCCTTCAGGGG

r and h indicate rat and human, respectively.
*Primers used for real-time PCR.

In the present study, using real-time polymerase chain reaction (PCR), we examined the expression level of all the components of the oxidase, including 5 Nox proteins (Nox1–5), in vascular endothelial cells. Furthermore, we investigated the superoxide-producing activity of the endothelial membranes using chemiluminescence and electron spin resonance (ESR).

Methods

Culture of Endothelial Cells

Rat aortic endothelial cells (RAECs) were collected from the aorta of male Sprague-Dawley rats (KYUDO Co Ltd, Tosu, Japan) 4 to 6 weeks old as described previously[2] and cultured with DMEM supplemented with 10% FBS (Invitrogen). Human umbilical vein endothelial cells (HUVECs) were purchased from Clonetics and were cultured with EGM-2 culture kit (Clonetics). Both cells at the 2nd to 7th passage were harvested with trypsinization and used for the following experiments.

Preparation of Neutrophils

Human neutrophils were isolated from venous blood of healthy volunteers by dextran sedimentation, hypotonic exposure, and the Ficoll-Paque method (Amersham Pharmacia Biotech) as described previously.[14]

Reverse Transcription–PCR

Total RNA was prepared with TRIzol reagent (Invitrogen). One microgram of total RNA was reverse-transcribed by AMV-transcriptase (Roche) in a total volume of 20 μL. Using 0.5 μL of the product as a template, PCR was performed with gene-specific primers as shown in Table 1.

Quantitative Real-Time PCR

The reverse transcriptase (RT) products (0.5 μL) were amplified with LightCycler (Roche) in the reaction mixture (20 μL) containing 2 μL of LightCycler-FastStart DNA Master SYBR Green I, 0.5 μmol/L of each primer, and 3 mmol/L $MgCl_2$. The mRNA levels were determined by quantitative real-time PCR performed twice for each of the independently prepared total RNAs. The numbers were standardized by those of 2 housekeeping genes, GAPDH and cyclophilin B.

Cell Fractionation

The endothelial cells and neutrophils were lysed by sonication in the presence of proteinase inhibitors, ie, 1 mmol/L PMSF, 1 μg/mL leupeptin, and 1 μg/mL pepstatin A, and the sonicate was centrifuged for 10 minutes at 10 000*g*. The resultant supernatant was centrifuged for 60 minutes at 100 000*g*. The pellet was defined as the membrane fraction and the supernatant as the cytosolic fraction.[9,14,20]

Plasmid Construction and Preparation of Recombinant Proteins

Plasmid constructions (pGEX-2T–p47phox, pGEX-2T–p67phox-N [amino acids 1 to 242], and pGEX-2T–Rac2 [Q61L]) were performed as described previously.[14] Proteins fused to GST were expressed in *Escherichia coli* strain BL21 and purified by glutathione–Sepharose-4B (Amersham Pharmacia Biotech).[14]

Superoxide Measurement by Chemiluminescence

Superoxide was measured by chemiluminescence with lucigenin (Sigma) or Diogenes (National Diagnostics) as described previously.[14,19,20] Briefly, the membranes (20 μg protein) were suspended in 100 mmol/L potassium phosphate, pH 7.0, containing 10 μmol/L FAD, 1 mmol/L EGTA, 1 mmol/L $MgCl_2$, 1 mmol/L NaN_3, and 5 μmol/L lucigenin or 50 μL Diogenes. After incubation of membranes for 1 minute with or without the recombinant proteins GST–p47phox, GST–p67phox-N, and GST–Rac2 (Q61L), in the presence of 100 μmol/L SDS at room temperature, 0.5 mmol/L NADPH was added to the reaction mixture.[14] The chemiluminescence was measured with a luminometer (MiniLumat LB9506; EG&G Berthold). The reaction was stopped by addition of superoxide dismutase (SOD; 200 U/mL).

Superoxide Measurement by ESR

ESR measurement was performed at room temperature with a JES-RE1X ESR spectrometer (JEOL). The setting conditions of the instrument were as follows: Magnetic field was 338.6±7.5 mT, modulation amplitude 0.1 mT, time constant 300 ms, modulation frequency 100 kHz, microwave power 10 mW, microwave frequency 9.425 GHz, and sweep time 8 minutes. Membrane protein (20 μg) was incubated with 10 mmol/L 5-(diethoxyphosphoryl)-5-methyl-1-pyrroline *N*-oxide (DEPMPO)[24] in 100 mmol/L potassium phosphate, pH 7.0, containing 10 μmol/L FAD, 1 mmol/L EGTA, 1 mmol/L $MgCl_2$, 1 mmol/L NaN_3, and indicated concentrations of NADPH or NADH in the presence or absence of the recombinant proteins and 100 μmol/L SDS in a total volume of 200 μL.

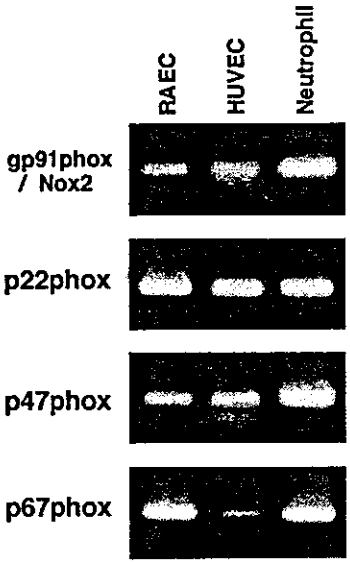

Figure 1. Expression of NAD(P)H oxidase components in RAECs, HUVECs and neutrophils. RT-PCR was performed using gene-specific primers (Table 1). PCR products were subjected to 1.2% agarose-gel electrophoresis and stained with ethidium bromide.

Antisense Transfection

Phosphorothioate oligonucleotides, including Nox4 antisense (5′-GGACACAGCCATGCCGCC-3′, sense (5′-GGCGGCATGG-CTGTGTCC-3′), scramble (5′-GGGTGAGGTCATCCTAGG-3′), previously reported[25] p22phox antisense (5′-GATCTGCCCCAT-GGTGAGGACC-3′), and p22phox sense (5′-GGTCCTCACCA-TGGGGCAGATC-3′), were prepared (Amersham-Pharmacia Biotech). Indicated concentrations of oligonucleotide and 1 μg of lipofectin (Invitrogen) per 1 μg oligonucleotide were diluted with Opti-MEM (Invitrogen) and incubated for 30 minutes, respectively. Then, the oligonucleotide and the lipofectin solutions were mixed and incubated for 15 minutes. The endothelial cells with 60% to 70% confluence were treated with the oligonucleotide/lipofectin mixture for 4 hours. After removing the mixture, the cells were incubated in DMEM with 10% FBS for 30 hours before the following experiments.

Superoxide Detection by Fluorescence Microscopy

The oxidative fluorescent dye dihydroethidium was used to evaluate superoxide production in vivo as described previously.[26] The endothelial cells on 35-mm glass-bottom dishes (MatTek) were treated with 10 μmol/L dihydroethidium for 20 minutes at 37°C. Ethidium fluorescence (excitation at 490 nm, emission at 610 nm) was examined by fluorescence microscopy (DM IRB, Leica).

Statistical Analysis

Values were expressed as mean±SEM. Results were compared by unpaired *t* test or 1-way factorial ANOVA followed by a post hoc Scheffé's comparison test. A value of $P<0.05$ was accepted as significant.

Results

Components of Oxidase in Endothelial Cells

Neutrophils highly expressed 2 membrane components, gp91phox/Nox2 and p22phox, and the specific cytosolic components p47phox and p67phox (Figure 1). The endothelial cells also expressed all of the 4 components; however, the expression levels of gp91phox/Nox2 and p47phox in both RAECs and HUVECs and that of p67phox in HUVECs were very limited (Figure 1). We used real-time PCR to quantify the expression number of each component. The real-time PCR disclosed that the expression numbers of gp91phox/Nox2 and p47phox were considerably lower than those of neutrophils (Table 2).

Because the expression level of gp91phox/Nox2 was quite low in the endothelial cells, we examined the expression of other Nox proteins (Nox1 and Nox3–5) in RAECs and HUVECs. Among the Nox proteins, Nox4 was highly expressed in the endothelial cells (Figure 2A). The expression number of Nox4 in the endothelial cells was estimated to be ≥10 000 copies per 25 mg of total RNA at a proliferating state by real-time PCR (Table 2). Expression of Nox1 was also detected in the endothelial cells, but the expression level was significantly lower (Figure 2A).[27]

Regulated Expression of Nox4 in Endothelial Cells

We examined whether the Nox4 expression was affected by culture conditions in the endothelial cells. When FBS was removed from culture medium for 24 hours, Nox4 expression was increased by 2- to 3-fold. Conversely, readdition of FBS suppressed the Nox4 expression to the basal level in 12 hours (Figure 2B). The change of p22phox expression after the removal and readdition of serum was almost in accordance with that of Nox4 (Figure 2C).

Superoxide-Producing Activity of Endothelial Membranes

Because Nox4 protein is speculated to exist in membranes by its structural similarity to gp91phox/Nox2,[19,20] we investigated whether the membrane fraction of RAECs was capable of producing superoxide. Addition of NADPH to the membrane fraction of RAECs promptly increased the chemiluminescence using a low concentration of lucigenin[16,18]; however, SOD did not abolish the signal[16] (data not shown). Conversely, an NADPH-induced increase of chemiluminescence by use of Diogenes was completely inhibited by SOD (Figure 3A), indicating that the Diogenes is more reliable for detection of superoxide. In this method, the superoxide-producing activity of RAEC membranes was almost equivalent to that of neutrophil membranes (data not shown). The

TABLE 2. Quantification of mRNA of the NADPH Oxidase Components by Real-Time PCR

	gp91phox/Nox2	p22phox	p47phox	p67phox	Nox4
RAECs	6.2±3.1	12 779.3±1740.2	1.5±0.5	2539.5±724.7	14 666.5±6975.6
HUVECs	3.3±1.7	877.8±197.9	2.5±0.9	41.8±13.5	16 961.3±2499.9
Neutrophils	191 117.0±60 046.5	81 082.5±14 508.1	151 639.2±54 698.9	76 299.3±16 960.6	10.2±3.5

RNA was prepared from the indicated cells, reverse-transcribed, and quantified by real-time PCR. Values (mean±SEM) are expressed as copy numbers (n=4), which are standardized by 2 housekeeping genes, GAPDH and cyclophilin B.

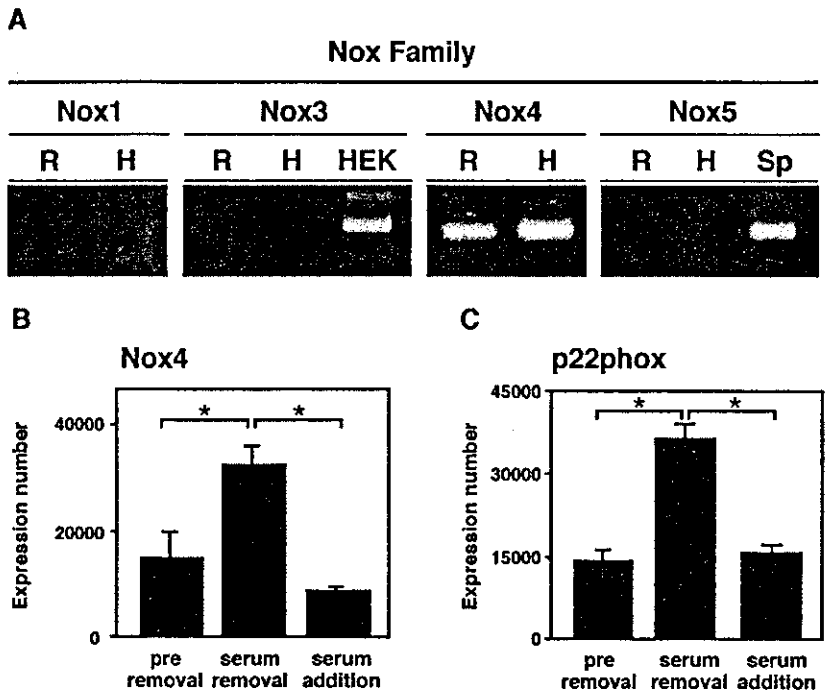

Figure 2. Regulated expression of Nox4 and p22phox by culture conditions. A, RT-PCR was performed using gene-specific primers (Table 1). R, H, HEK, and Sp indicate RAECs, HUVECs, HEK293 cells, and rat spleen, respectively. Both HEK293 and spleen were used for positive controls for primers. B and C, Expression changes of Nox4 (B) and p22phox (C) in RAECs after serum removal for 24 hours and readdition for 12 hours were determined by real-time PCR (n=4; *P<0.05).

NADPH-induced increases of chemiluminescence in both RAEC and neutrophil membranes were inhibited by 10 μmol/L diphenylene iodonium but not by 100 μmol/L N^G-nitro-L-arginine methyl ester, 100 μmol/L indomethacin, and 100 μmol/L oxypurinol (data not shown). Furthermore, we used ESR to show that the RAEC membranes produced both superoxide (DEPMPO-OOH adduct) and hydroxyl radical (DEPMPO-OH adduct) in a NADPH-dependent manner (Figure 3B). Addition of SOD (Figure 3B) but not catalase (data not shown) completely inhibited both signals, indicating that hydroxyl radical was derived from superoxide.[28] The total amount of superoxide and hydroxyl radical produced by RAEC membranes was almost equivalent to that of the unstimulated neutrophil membranes (Figures 3B, 3C, and 4C). The effects of NADH on the activity of the endothelial NAD(P)H oxidase were almost similar to those of NADPH, and the effect of each substrate was dependent on its concentration (data not shown).

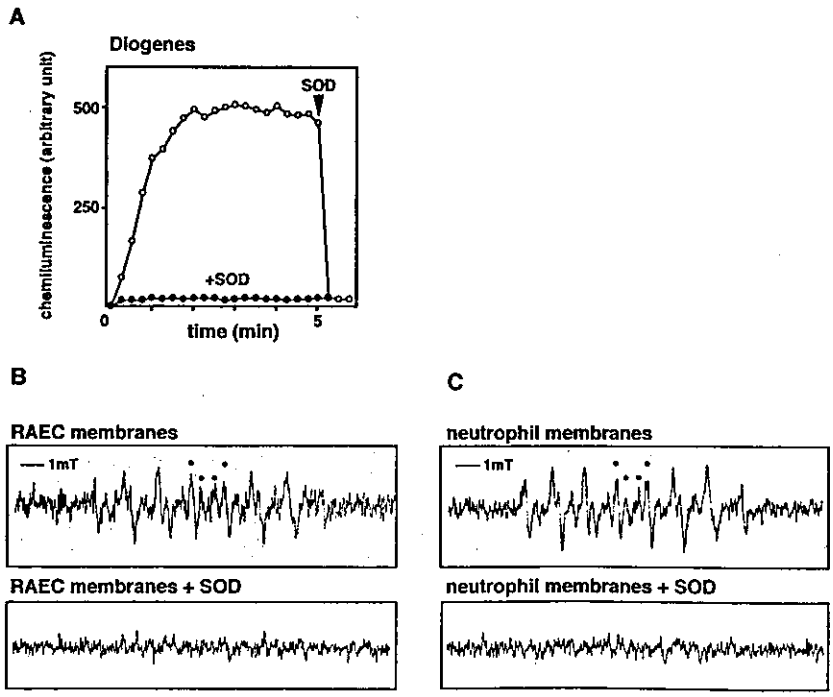

Figure 3. Superoxide-producing activity of endothelial membranes. A, RAEC membranes were stimulated with 0.5 mmol/L NADPH under conditions described in Methods. Changes in chemiluminescence with Diogenes were monitored continuously. Where indicated, 200 U/mL SOD was added. B and C, ESR detection of DEPMPO spin adducts from RAECs (B) and unstimulated neutrophil membranes (C). DEPMPO-OOH (open circle) and DEPMPO-OH (closed circle) obtained by incubating membranes with 0.5 mmol/L NADPH for 1 hour were indicated. Signals were inhibited by coincubation with 200 U/mL SOD.

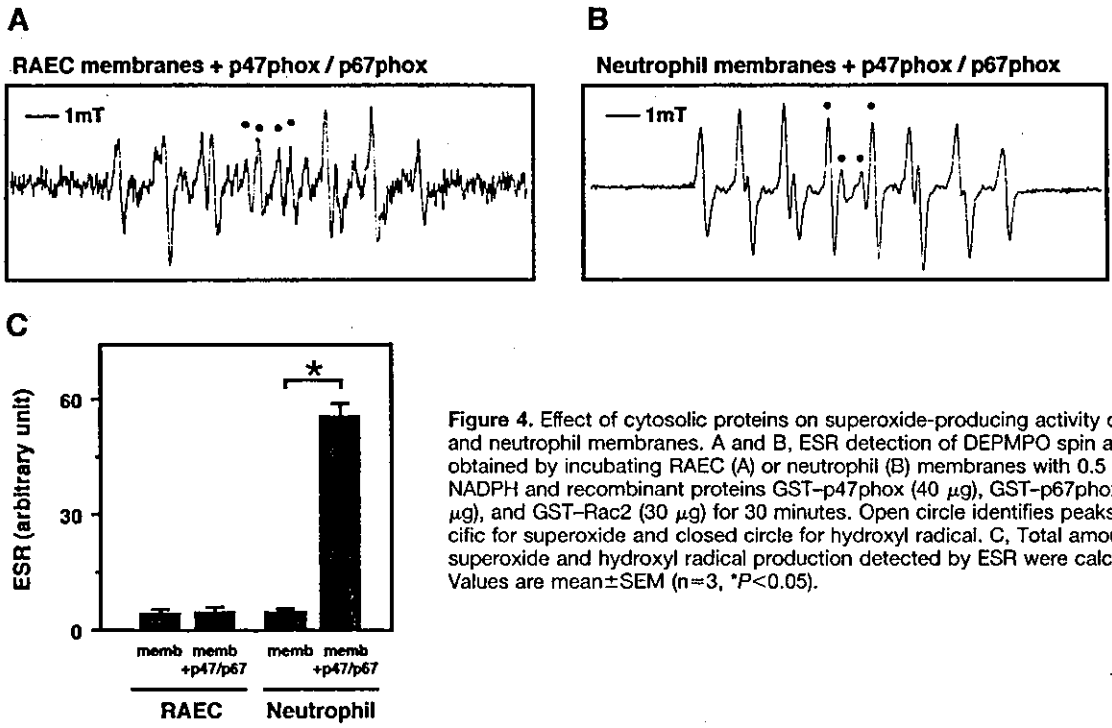

Figure 4. Effect of cytosolic proteins on superoxide-producing activity of RAEC and neutrophil membranes. A and B, ESR detection of DEPMPO spin adducts obtained by incubating RAEC (A) or neutrophil (B) membranes with 0.5 mmol/L NADPH and recombinant proteins GST-p47phox (40 μg), GST-p67phox (40 μg), and GST-Rac2 (30 μg) for 30 minutes. Open circle identifies peaks specific for superoxide and closed circle for hydroxyl radical. C, Total amounts of superoxide and hydroxyl radical production detected by ESR were calculated. Values are mean±SEM (n=3, *P<0.05).

Role of the Cytosolic Components p47phox and p67phox in Endothelial Cells

To examine the activity of the cytosolic factors, we prepared 3 recombinant proteins, GST-p47phox, GST-p67phox, and GST-Rac2. When the recombinant proteins were added to the neutrophil membranes, the typical DEPMPO-OOH adduct was readily detected and was estimated to be ≈10-fold higher than that of the membranes alone (Figure 4, B and C). When the recombinant proteins were added to RAEC membranes, ESR signals were almost similar to those of RAEC membranes alone (Figure 4, A and C). We obtained similar results by the cell-free system using Diogenes (data not shown).

Nox4 Is Involved in Superoxide Production in Endothelial Cells

To elucidate whether Nox4 is involved in the endothelial superoxide production, we used a Nox4 antisense oligonucleotide. The Nox4 antisense oligonucleotide significantly suppressed Nox4 expression in a concentration-dependent manner (Figure 5A) but did not affect the expression of gp91phox/Nox2 at all (data not shown). Using fluorescent microscopy, we confirmed that intracellular superoxide production was decreased in accordance with antisense oligonucleotide-dependent suppression of Nox4 (Figure 5B). Furthermore, to quantify the reduction of superoxide production by the oligonucleotides, we performed the chemiluminescence experiment using membrane fractions treated with the oligonucleotides. The superoxide-producing activity of the membrane fractions treated with the Nox4 antisense oligonucleotide was significantly smaller than that treated with sense or scramble oligonucleotide (Figure 5C). The degree of reduction in superoxide production by the Nox4 antisense (≈50%) was coincident with the inhibitory effect on the Nox4 mRNA by the Nox4 antisense. A p22phox antisense oligonucleotide similarly reduced the superoxide production of the endothelial membranes by 40% to 50% (Figure 5C).

Discussion

Here, we demonstrated a new finding that Nox4 may function as the major catalytic component of an endothelial NAD(P)H oxidase.

Presence of Nox4 in Endothelial Cells

In the present study, we have confirmed, using RT-PCR, that Nox4 is abundantly expressed in both RAECs and HUVECs. The expression level determined by real-time PCR was comparable to that of vascular muscle cells, which had already been established as Nox4-expressing cells.[23,29] Moreover, the activity of the endothelial NAD(P)H oxidase was similar with Nox4-containing oxidase.[20] The endothelial membranes produced an amount of superoxide comparable to that of the unstimulated neutrophil membranes. However, the oxidase activity of the endothelial membranes was not enhanced significantly by the cytosolic proteins p47phox and p67phox.[20] The NAD(P)H-dependent superoxide production in the endothelial cells was inhibited by diphenylene iodonium, an inhibitor of flavoproteins, but not by other inhibitors, such as N^G-nitro-L-arginine methyl ester, indomethacin, and oxypurinol, suggesting that the superoxide production was derived from Nox family proteins. We have also shown that Nox4 suppression by a Nox4 antisense oligonucleotide is coincident with the reduction of the superoxide-producing activity of the endothelial membranes. In addition, the effect of a p22phox antisense oligonucleotide on superoxide production in endothelial membranes was comparable to that of the Nox4 antisense. These findings suggest that Nox4 may be

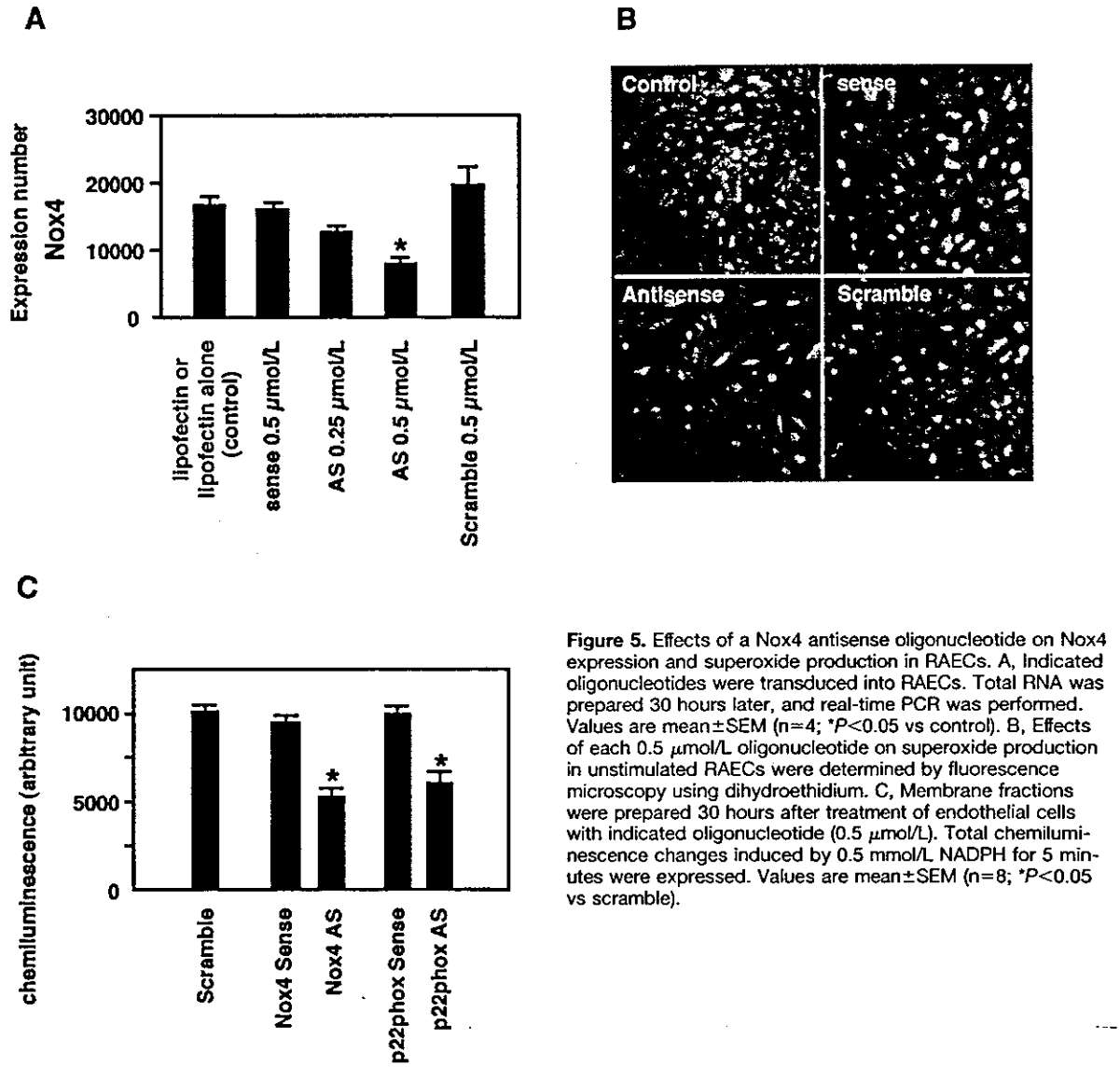

Figure 5. Effects of a Nox4 antisense oligonucleotide on Nox4 expression and superoxide production in RAECs. A, Indicated oligonucleotides were transduced into RAECs. Total RNA was prepared 30 hours later, and real-time PCR was performed. Values are mean±SEM (n=4; *$P<0.05$ vs control). B, Effects of each 0.5 μmol/L oligonucleotide on superoxide production in unstimulated RAECs were determined by fluorescence microscopy using dihydroethidium. C, Membrane fractions were prepared 30 hours after treatment of endothelial cells with indicated oligonucleotide (0.5 μmol/L). Total chemiluminescence changes induced by 0.5 mmol/L NADPH for 5 minutes were expressed. Values are mean±SEM (n=8; *$P<0.05$ vs scramble).

present and functionally active with p22phox as a superoxide-producing enzyme in the endothelial cells. Sorescu et al[27] also recently reported that Nox4 is abundantly expressed in cultured endothelial cells. We also cannot exclude the possibility that the residual activity is derived from other superoxide-producing enzymes, such as gp91phox/Nox2, as described below.

Presence of Multiple Nox Proteins in Endothelial Cells

It is well established that gp91phox/Nox2 is expressed in endothelial cells.[17,18] In the present study, we also found that a small but significant amount of gp91phox/Nox2 is expressed in both RAECs and HUVECs. It was reported that Nox1 and Nox4 are coexpressed in vascular muscle cells.[23] Thus, Nox4 as well as gp91phox/Nox2 may function as a superoxide-producing enzyme in the endothelial cells. Although all Nox proteins (Nox1–5) are considered to be involved in superoxide production,[10,19,20,22] it remains poorly understood how cells deal with distinct Nox proteins. A possible explanation may be that intracellular localization of each Nox protein is different, which may determine the role of each Nox protein.[19,23] gp91phox/Nox2 is established to exist in the plasma or granular membranes of neutrophils. By use of the PSORT program, it is predicted that Nox4 may be localized in endoplasmic reticulum.[23] Thus, it may be possible that Nox4 and gp91phox/Nox2 are expressed in the distinct membrane of the endothelial cells and have different roles in the cell functions.

It has been reported that gp91phox/Nox2 and p22phox stabilize each other at the protein level.[12] Because the expression of p22phox was much higher than that of gp91phox/Nox2 in endothelial cells,[17] one might anticipate that p22phox could not exist stably at the protein level. Lassegue et al[23] suggested that both Nox1 and Nox4 may form complexes with p22phox and compose functional cytochromes in vascular muscle cells. Thus, it may be possible that Nox4 as well as gp91phox/Nox2 may form a complex with p22phox in endothelial cells.

Role of Nox4 in Endothelial Cells

Nox4 was originally identified from kidney, where Nox4 probably serves as an oxygen sensor to regulate the production of erythropoietin.[19,20] Thereafter, it was disclosed that Nox4 is expressed in many tissues, including vascular muscle cells.[21,23] In atherosclerotic lesions,[27,29] Nox4 was highly expressed with Nox1 and p22phox and produced superoxide, suggesting that Nox4 may play some important role in formation of atherosclerotic lesions. Furthermore, it has been reported that Nox4 expression is decreased by proliferative stimuli, such as angiotensin II, platelet-derived growth factor, and serum, in cultured vascular muscle cells.[23] In the present study, the Nox4 expression in endothelial cells was significantly increased with the suppression of cell proliferation by serum removal and decreased by addition of serum. Taken together with the previous observation that overexpression of Nox4 in fibroblast NIH 3T3 cells decreased the rate of proliferation of the cells,[19,20] it is possible that Nox4 plays a role in the regulation of cell growth or cell survival in endothelial cells.

In conclusion, we provide here several lines of evidence that Nox4 functions as an important membrane component of an endothelial NAD(P)H oxidase along with the oxidase consisting of gp91phox/Nox2.

References

1. Kitazono T, Ibayashi S, Nagao T, et al. Role of tyrosine kinase in dilator responses of rat basilar artery in vivo. *Hypertension.* 1998;31:861–865.
2. Kitayama J, Kitazono T, Ibayashi S, et al. Role of phosphatidylinositol 3-kinase in acetylcholine-induced dilatation of rat basilar artery. *Stroke.* 2000;31:2487–2493.
3. Cai H, Harrison DG. Endothelial dysfunction in cardiovascular diseases: the role of oxidant stress. *Circ Res.* 2000;87:840–844.
4. Griendling KK, Sorescu D, Ushio-Fukai M. NAD(P)H oxidase: role in cardiovascular biology and disease. *Circ Res.* 2000;86:494–501.
5. Griendling KK, Sorescu D, Lassegue B, et al. Modulation of protein kinase activity and gene expression by reactive oxygen species and their role in vascular physiology and pathophysiology. *Arterioscler Thromb Vasc Biol.* 2000;20:2175–2183.
6. Mohazzab KM, Kaminski PM, Wolin MS. NADH oxidoreductase is a major source of superoxide anion in bovine coronary artery endothelium. *Am J Physiol.* 1994;266:H2568–H2572.
7. Griendling KK, Minieri CA, Ollerenshaw JD, et al. Angiotensin II stimulates NADH and NADPH oxidase activity in cultured vascular smooth muscle cells. *Circ Res.* 1994;74:1141–1148.
8. Pagano PJ, Clark JK, Cifuentes-Pagano ME, et al. Localization of a constitutively active, phagocyte-like NADPH oxidase in rabbit aortic adventitia: enhancement by angiotensin II. *Proc Natl Acad Sci U S A.* 1997;94:14483–14488.
9. Souza HP, Laurindo FR, Ziegelstein RC, et al. Vascular NAD(P)H oxidase is distinct from the phagocytic enzyme and modulates vascular reactivity control. *Am J Physiol.* 2001;280:H658–H667.
10. Suh YA, Arnold RS, Lassegue B, et al. Cell transformation by the superoxide-generating oxidase Mox1. *Nature.* 1999;401:79–82.
11. Ushio-Fukai M, Zafari AM, Fukui T, et al. p22phox is a critical component of the superoxide-generating NADH/NADPH oxidase system and regulates angiotensin II–induced hypertrophy in vascular smooth muscle cells. *J Biol Chem.* 1996;271:23317–23321.
12. Babior BM. NADPH oxidase: an update. *Blood.* 1999;93:1464–1476.
13. Roos D, de Boer M, Kuribayashi F, et al. Mutations in the X-linked and autosomal recessive forms of chronic granulomatous disease. *Blood.* 1996;87:1663–1681.
14. Ago T, Nunoi H, Ito T, et al. Mechanism for phosphorylation-induced activation of the phagocyte NADPH oxidase protein p47phox. Triple replacement of serines 303, 304, and 328 with aspartates disrupts the SH3 domain-mediated intramolecular interaction in p47phox, thereby activating the oxidase. *J Biol Chem.* 1999;274:33644–33653.
15. Ago T, Kuribayashi F, Hiroaki H, et al. Phosphorylation of p47phox directs phox homology domain from SH3 domain toward phosphoinositides, leading to phagocyte NADPH oxidase activation. *Proc Natl Acad Sci U S A.* 2003;100:4474–4479.
16. Jones SA, O'Donnell VB, Wood JD, et al. Expression of phagocyte NADPH oxidase components in human endothelial cells. *Am J Physiol.* 1996;271:H1626–H1634.
17. Bayraktutan U, Draper N, Lang D, et al. Expression of functional neutrophil-type NADPH oxidase in cultured rat coronary microvascular endothelial cells. *Cardiovasc Res.* 1998;38:256–262.
18. Li JM, Shah AM. Intracellular localization and preassembly of the NADPH oxidase complex in cultured endothelial cells. *J Biol Chem.* 2002;277:19952–19960.
19. Geiszt M, Kopp JB, Varnai P, et al. Identification of renox, an NAD(P)H oxidase in kidney. *Proc Natl Acad Sci U S A.* 2000;97:8010–8014.
20. Shiose A, Kuroda J, Tsuruya K, et al. A novel superoxide-producing NAD(P)H oxidase in kidney. *J Biol Chem.* 2001;276:1417–1423.
21. Cheng G, Cao Z, Xu X, et al. Homologs of gp91phox: cloning and tissue expression of Nox3, Nox4, and Nox5. *Gene.* 2001;269:131–140.
22. Banfi B, Molnar G, Maturana A, et al. A Ca^{2+}-activated NADPH oxidase in testis, spleen, and lymph nodes. *J Biol Chem.* 2001;276:37594–37601.
23. Lassegue B, Sorescu D, Szocs K, et al. Novel gp91(phox) homologues in vascular smooth muscle cells: nox1 mediates angiotensin II–induced superoxide formation and redox-sensitive signaling pathways. *Circ Res.* 2001;88:888–894.
24. Frejaville C, Karoui H, Tuccio B, et al. 5-(Diethoxyphosphoryl)-5-methyl-1-pyrroline *N*-oxide: a new efficient phosphorylated nitrone for the in vitro and in vivo spin trapping of oxygen-centered radicals. *J Med Chem.* 1995;38:258–265.
25. Lynn S, Gurr JR, Lai HT, et al. NADH oxidase activation is involved in arsenite-induced oxidative DNA damage in human vascular smooth muscle cells. *Circ Res.* 2000;86:514–519.
26. Miller FJ Jr, Gutterman DD, Rios CD, et al. Superoxide production in vascular smooth muscle contributes to oxidative stress and impaired relaxation in atherosclerosis. *Circ Res.* 1998;82:1298–1305.
27. Sorescu D, Weiss D, Lassegue B, et al. Superoxide production and expression of nox family proteins in human atherosclerosis. *Circulation.* 2002;105:1429–1435.
28. Souza HP, Liu X, Samouilov A, et al. Quantitation of superoxide generation and substrate utilization by vascular NAD(P)H oxidase. *Am J Physiol.* 2002;282:H466–H474.
29. Szocs K, Lassegue B, Sorescu D, et al. Upregulation of Nox-based NAD(P)H oxidases in restenosis after carotid injury. *Arterioscler Thromb Vasc Biol.* 2002;22:21–27.

Diagnostic Impact of Transcranial Color-Coded Real-Time Sonography With Echo Contrast Agents for Hyperperfusion Syndrome After Carotid Endarterectomy

Shigeru Fujimoto, MD; Kazunori Toyoda, MD; Tooru Inoue, MD; Yuko Hirai, MD; Takeshi Uwatoko, MD; Kazuhiro Kishikawa, MD; Kotaro Yasumori, MD; Setsuro Ibayashi, MD; Mitsuo Iida, MD; Yasushi Okada, MD

Background and Purpose—The purpose of the present study was to evaluate availability of transcranial color-coded real-time sonography (TCCS) to detect hyperperfusion after carotid endarterectomy (CEA).

Methods—This prospective study included 105 consecutive patients who underwent CEA for severe carotid stenosis. TCCS with echo contrast agents was performed serially to evaluate flow velocity of the middle cerebral artery (MCA). Regional cerebral blood flow (rCBF) and vasodilatory capacity of the MCA territory were evaluated using single-photon emission computed tomography. We compared the changes in MCA flow velocity with rCBF.

Results—Using echo contrast agents, we could evaluate the MCA flow in 95 (90%) of 105 patients. Twelve patients showed hyperperfusion syndrome. Changes in the MCA mean flow velocity (MFV) before and 4 days after CEA were significantly correlated with those in rCBF (r=0.48; P<0.0001). An increase of >50% in MCA MFV was observed within 4 days after CEA in all 12 patients with hyperperfusion syndrome. Multivariate analysis revealed that reduced vasodilatory capacity (odds ratio, 0.14; 95% CI, 0.04 to 0.46) was an independent risk factor for a 1.5-fold increase in the MFV of MCA ipsilateral to CEA.

Conclusions—Findings of a 1.5-fold increase in the MCA MFV can accurately identify those patients with high risk of developing post-CEA hyperperfusion syndrome. TCCS with echo contrast agents is available for the evaluation of hyperperfusion after CEA. (*Stroke*. 2004;35:1852-1856.)

Key Words: carotid endarterectomy ■ cerebral blood flow ■ ultrasonography, Doppler, transcranial ■ contrast media

Hyperperfusion syndrome is well known as a significant complication after carotid endarterectomy (CEA). In previous studies, hyperperfusion syndrome was not shown to be frequent, but it was found to be fatal once an intracranial hemorrhage occurred.[1,2] Thus, frequent evaluations of cerebral hemodynamics after CEA are required to watch for development of the syndrome. Because single-photon emission computed tomography (SPECT) and positron emission tomography for the measurement of regional cerebral blood flow (rCBF) are expensive, complicated, and time consuming, they may not be the appropriate modalities to use repeatedly after CEA.

Several studies have demonstrated the usefulness of transcranial Doppler (TCD) to monitor the flow velocity of the middle cerebral artery (MCA) after CEA and thus to predict the occurrence of hyperperfusion syndrome.[3–6] However, the accuracy of TCD for measuring MCA flow velocity remained controversial. One can more readily and confidently identify particular vascular structure with transcranial color-coded real-time sonography (TCCS) than with TCD.[7,8] A limiting factor in TCCS use as a screening tool is its relatively low sensitivity in detecting intracranial arteries (≈60% to 70%) because of an inadequate temporal bone window, especially in elderly patients.[7,8] However, echo contrast agents have improved the quality of TCCS significantly.[9,10]

The purpose of this study was to evaluate the availability and accuracy of MCA flow velocity as measured by TCCS with echo contrast agents in detecting hemispheric hyperperfusion syndrome after CEA.

Subjects and Methods

Patients

A total of 105 consecutive patients who underwent CEA for carotid stenosis in our Cerebrovascular Center from September 2001 to September 2003 were included prospectively in the study. All patients gave informed consent to undergo cerebral angiography and CEA.

Received January 22, 2004; final revision received April 6, 2004; accepted May 4, 2004.

From the Departments of Cerebrovascular Disease (S.F., K.T., Y.H., T.U., K.K., Y.O.), Neurosurgery (T.I.), and Neuroradiology (K.Y.), Cerebrovascular Center and Clinical Research Institute, National Kyushu Medical Center, Fukuoka, Japan; and the Department of Medicine and Clinical Science (S.I., M.I.), Graduate School of Medical Science, Kyushu University, Fukuoka, Japan.

Correspondence to Dr Shigeru Fujimoto, Department of Cerebrovascular Disease and Clinical Research Institute, National Kyushu Medical Center, 1-8-1 Jigyohama, Chuo-ku, Fukuoka 810-8563, Japan. E-mail fujimoto@qmed.hosp.go.jp

Stroke is available at http://www.strokeaha.org

DOI: 10.1161/01.STR.0000133131.93900.ff

In accordance with American Heart Association guidelines,[11] we adopted the following criteria as indications for CEA: (1) carotid stenosis of ≥70%, or 50% to 69% with repeated ischemic cerebrovascular events or severe ulcerative atheroma; (2) modified Rankin scale of ≤2; (3) small or no brain infarction on MRI; and (4) absence of significant occlusive disease (≥70% in diameter) distal to the carotid stenosis. The degree of carotid stenosis was assessed using cerebral digital subtraction angiography with the method documented in the North American Symptomatic Carotid Endarterectomy Trial (NASCET) study.[12] Six patients underwent bilateral CEA. The second CEA was performed 0.9 to 8.4 months (mean 4.3 months) after the first CEA.

Surgical Procedure

All CEA procedures were performed by the same neurosurgical team. Endarterectomy was performed using a microscope. After CEA, propofol sedation was continued until the next morning. Blood pressure was controlled using nitroglycerin and/or diltiazem until 7 days after CEA so that it was <150 mm Hg systolic and 90 mm Hg diastolic in all patients.

Clinical Diagnosis of Hyperperfusion Syndrome

After CEA, clinical and neurological symptoms were observed. Probable hyperperfusion syndrome was diagnosed if the patient demonstrated a focal seizure, temporary deterioration of consciousness level with remarkably abnormal speech and conduct for >6 hours after stopping propofol sedation, development of focal neurological signs such as motor weakness, or intracranial hemorrhage on computed tomography (CT). Temporary consciousness level deterioration within 6 hours after stopping anesthesia and sedation was regarded as an anesthetic effect. If a patient was diagnosed as having a hyperperfusion syndrome, cranial CT and MRI studies were performed immediately. All patients underwent MRI 14 days after CEA. After CEA, blood pressure was also monitored in all patients. An increase in blood pressure was a reference criterion for the diagnosis of hyperperfusion syndrome. When a remarkable increase in blood pressure occurred within 7 days after CEA, CT studies were performed to evaluate whether ischemic or hemorrhagic changes were shown. Clinical diagnosis of hyperperfusion syndrome was done by a neurosurgeon who was blinded to TCCS findings.

TCCS Studies

A commercially available real-time 2D TCCS system (model HDI-5000; ATL Ultrasound) with a 2.5-MHz transducer for B-mode imaging and Doppler functions was used. The transducer was placed on the temporal surface. Particular care was taken to display a long-axis view of the horizontal portion of the MCA as a color flow on the B-mode image. Range-gated pulsed Doppler ultrasound with a sample volume length of 2 mm was used to measure MCA blood flow velocity. The incident angle between MCA and the Doppler beam was kept at ≤60°. Absolute values of peak systolic, end diastolic, and mean flow velocity (MFV) of ipsilateral or bilateral MCAs were measured using the maximum frequency envelope. TCCS studies were performed serially before, 1 hour, 1 day, 4 days, and 7 days after CEA. When ipsilateral MCA flow could not be displayed because of an inadequate temporal bone window, TCCS studies were repeated after intravenous echo contrast agent administration (300 mg/mL of Levovist; Schering).

Changes in MCA MFV were expressed using the following equation: MFV ratio=MFV after CEA/MFV before CEA.

Carotid Ultrasonography

Before CEA, conventional carotid duplex ultrasonography was performed to evaluate the carotid stenosis grade. The HDI-5000 with the 12-to-5–MHz linear array transducer was used. The maximum area and linear percent stenosis were measured. Transoral carotid ultrasonography (TOCU) was also performed to evaluate the portion distal to the carotid stenosis before and 2 weeks after CEA according to a method described previously.[13,14] A 9-to-5–MHz convex array transducer was used. The diameter and flow velocity of the extracranial internal carotid artery (ICA) were measured at the nearest point from the surface of the posterior pharyngeal wall.

SPECT Studies

Cerebral hemodynamics were evaluated using SPECT before, 4 days after, and 14 days after CEA. The SPECT apparatus was the PRISM 2000X (2-head SPECT system; Picker), and ^{99m}Tc-ethyl cysteinate dimmer was used as the tracer. An elliptical region of interest (ROI) >16 cm^2 in size was located in the cortical area in the MCA territory of each side. Areas of infarct, if present, were excluded from the ROI. rCBF values were measured quantitatively using the Patlack plot method[15,16] before, 4 days after, and 14 days after CEA. rCBF values were also measured after the acetazolamide (ACZ) challenge test before and 14 days after CEA. Vasodilatory capacity (ACZ reactivity) was expressed using the following equation: ACZ reactivity=[(post-ACZ CBF−resting rCBF)/resting rCBF]×100. ACZ reactivity was classified into 3 groups: remarkably reduced ACZ reactivity (group A; ≤10%); slightly reduced ACZ reactivity (group B; >10% and <20%); and normal ACZ reactivity (group C; ≥20%).

Changes in rCBF of the MCA territory were expressed using the following equation: CBF ratio=rCBF after CEA/rCBF before CEA.

Data Analysis

The relationships between the occurrence of a hyperperfusion syndrome and changes in MCA flow velocities after CEA were investigated. Clinical and radiological factors that could predict the occurrence of hyperperfusion syndrome after CEA were also studied. For univariate analysis, the χ^2 test, paired t test, and 2-way repeated-measures ANOVA were used. Linear-regression analysis and the Pearson correlation coefficient were used to evaluate the correlation between changes in MCA territory CBF and MCA flow velocity. Logistic regression analysis was done for multivariate analysis. A P value of <0.05 was considered significant.

Results

Patient Demographics

Ninety men and 15 women aged 68.4±7.4 (mean±SD) years were included. Carotid lesions were symptomatic in 67 patients (64%) and asymptomatic in 38 (36%). The National Institutes of Health Stroke Scale (NIHSS) scores for symptomatic patients ranged between 1 and 10 (median 3). The carotid stenosis grade as determined by the NASCET method was 79.7±14.3%.

MCA Flow Detection by TCCS

Because of an insufficient temporal bone window, ipsilateral MCA flows were invisible with conventional TCCS in 38 (36%) of 105 patients. In these 38 patients, 28 additional MCA flows could be observed by TCCS using echo contrast agents. Therefore, the sensitivity of the method for detecting an MCA flow was 90% (95 of 105). All 95 patients were included in the data analysis.

Clinical Observations

No complications were observed during CEA procedures. After propofol sedation was stopped the morning after CEA, focal seizures were present in 3 patients (3%), and temporary deterioration of consciousness level with remarkably abnormal speech and conduct occurred in 9 patients (9%). Among 6 patients with bilateral CEA, 1 had hyperperfusion syndrome after the second CEA. Of the 95 patients, 12 patients (13%) were suspected to have hyperperfusion syndrome. The syndrome occurred on the first postsurgical day for 8 patients, the second day for 2, the fourth day for 1, and the fifth day for 1.

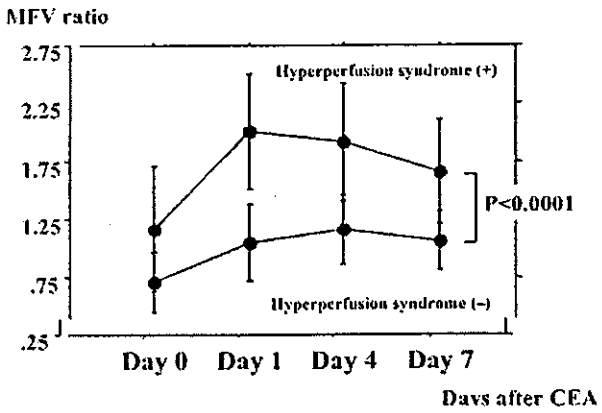

Figure 1. Changes in MCA MFV ratio in patients with (+) and without (−) hyperperfusion syndrome.

No new hemorrhagic or ischemic lesions were detected in any patients during cranial CT or MRI within 4 days after CEA and MRI 14 days after CEA. Although 2 patients with focal seizure had hyperintense area in the ipsilateral parieto-occipital cortex on diffusion-weighted MRI just after the onset of the symptom, it disappeared after a 14-day follow-up MRI. Postsurgical blood pressure was somewhat high in patients with hyperperfusion syndrome compared with patients without hyperperfusion 1 hour after (127±17/64±8 versus 118±19/59±9 mm Hg), 1 day after (149±20/72±9 versus 136±25/63±13 mm Hg), 4 days after (151±15/79±11 versus 136±14/72±10 mm Hg), and 7 days after (147±21/71±14 versus 140±13/68±9 mm Hg) CEA.

Changes in MCA Flow Velocity and CBF in MCA Territory

MCA MFV increased significantly in the 12 patients with hyperperfusion syndromes 1 day after CEA (89.6±28.6 cm/s) compared with before the procedure (48.6±12.9 cm/s; $P<0.0001$). On the other hand, MCA MFV did not increase in the remaining 83 patients (from 60.0±13.0 cm/s to 62.8±20.3 cm/s). MCA MFV was lower in patients with hyperperfusion syndrome than without before CEA (48.6±12.9 versus 60.0±13.0 cm/s; $P<0.001$) and higher 1 day after CEA (89.6±28.6 versus 62.8±20.3 cm/s; $P<0.05$). In patients with hyperperfusion syndrome, the post-CEA MFV ratio was significantly higher than in patients without hyperperfusion ($P<0.0001$), with a peak in the ratio occurring 1 day after CEA (2.01±0.49; Figure 1).

Furthermore, in the 12 patients with post-CEA hyperperfusion syndrome, the CBF ratio 4 days after CEA was higher than in the 83 patients without hyperperfusion (1.24±0.11 versus 1.07±0.10; $P<0.0001$). There was no significant difference in CBF ratio 14 days after CEA between patients with and patients without hyperperfusion syndrome (1.06±0.15 versus 1.06±0.13). Of note, 4 days after CEA, MFV ratio was significantly correlated with CBF ratio ($r=0.48$; $P<0.0001$; Figure 2).

Relationships Between Hyperperfusion Syndrome and MFV Ratio

One day after CEA, 10 of 12 patients with hyperperfusion syndrome showed an MFV ratio of ≥1.5 (Figure 3). In these

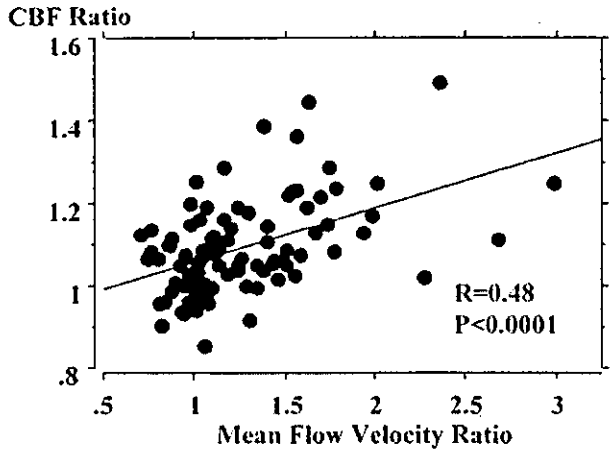

Figure 2. Correlation between changes in rCBF in the MCA territory and MCA flow velocity 4 days after CEA.

10 patients, hyperperfusion syndrome occurred between 1 and 4 days after CEA. The remaining 2 patients had an MFV ratio between 1.4 and 1.5 1 day after CEA and >1.5 4 days after CEA. Both patients developed hyperperfusion syndrome between 4 and 7 days after CEA. Thus, a maximum MFV ratio of 1.5 within 4 postsurgical days was an appropriate cut-off value for the prediction of hyperperfusion syndrome. This cut-off yielded a sensitivity of 100% and a high specificity (84%). In the following analyses, we used this cut-off value as a hyperperfusion syndrome predictor.

Clinical, Radiological, and Ultrasonographical Findings and Increase in MFV in MCA

We examined the relationship of a maximum MFV ratio of ≥1.5 documented within 4 days after CEA as the optimal criterion for predicting postsurgical hyperperfusion syndrome and the clinical, radiological, and ultrasonographical data obtained before CEA. The following factors contributed to a prediction of the ratio >1.5: symptomatic carotid stenosis ($P<0.01$); NIHSS score ($P<0.01$); severe carotid stenosis using NASCET method ($P<0.01$); retrograde flow of the ophthalmic artery ipsilateral to the CEA detected by cerebral angiography

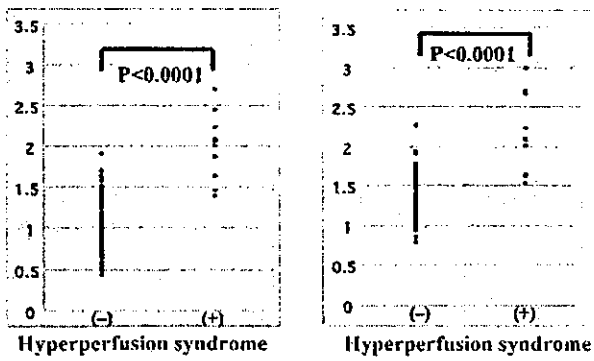

Figure 3. Relationships between occurrence of hyperperfusion syndrome and changes in MCA flow velocity. Left, MFV ratio value 1 day after CEA. Right, Maximum MFV ratio value between days 0 and 4.

TABLE 1. Clinical Factors to Predict Significant Increase in MCA Flow Velocity

	Maximum MFV Ratio		
	≥1.5 (n=25)	<1.5 (n=70)	*P*
Age, y	67.8±7.8	68.6±7.2	NS
Symptomatic	4 (16%)	6 (9%)	<0.01
NIHSS score	1.84±2.85	0.67±1.77	<0.01
Hypertension	22 (88%)	59 (84%)	NS
Diabetes mellitus	10 (40%)	23 (33%)	NS
Hyperlipidemia	11 (44%)	24 (34%)	NS
Ischemic heart disease	9 (40%)	20 (29%)	NS
Carotid stenosis, %			
NASCET (angiogram)	87.1±14.5	77.3±13.4	<0.001
Area (ultrasonography)	92.9±6.0	89.4±8.1	NS
Linear (ultrasonography)	79.1±12.4	75.7±9.6	NS

($P<0.0001$); MFV of the ipsilateral distal ICA by TOCU ($P<0.01$) and MCA by TCCS ($P<0.001$); small diameter of the ipsilateral distal ICA by TOCU ($P<0.01$); and rCBF ($P<0.05$) and ACZ reactivity ($P<0.001$) in the ipsilateral MCA territories (Tables 1 and 2). Furthermore, depending on the grade of ACZ reactivity, there was a significant difference in the maximum MFV ratio ($P<0.001$; Figure 4).

Multivariate analysis was done on the above factors that had a statistically significant relationship with a maximum MFV ratio of ≥1.5 within 4 days after CEA. It was shown that the actual grade (A through C) of the reduced ACZ reactivity was an independent predictor for hyperperfusion syndrome (odds ratio, 0.14; 95% CI, 0.04 to 0.46).

Discussion

This is the first report that has evaluated TCCS accuracy for detecting hyperperfusion syndrome and determined the correlation between quantitatively measured flow velocity and CBF. This study resulted in 3 major findings. First, MFV of the MCA ipsilateral to CEA obtained using TCCS was able to detect hemispheric hyperperfusion syndrome after CEA. Second, a >1.5-fold increase in the MFV within 4 postsurgical days was a predictor of hyperperfusion syndrome and had complete sensitivity with high specificity. Third, as important evidence for prediction of hyperperfusion using MFV, the postsurgical MFV ratio significantly correlated with postsurgical CBF and presurgical ACZ reactivity in the affected MCA territory as assessed by SPECT.

TABLE 2. Radiological and Ultrasonographical Findings Before CEA to Predict Significant Increase in MCA Flow Velocity

	Maximum MFV Ratio		
	≥1.5 (n=25)	<1.5 (n=70)	*P*
Angiographical findings			
Contralateral vascular lesions			
≥70% in NASCET method	4 (16%)	6 (9%)	NS
Retrograde flow of ipsilateral			
Ophthalmic artery	18 (72%)	19 (27%)	<0.0001
TOCU findings (distal ICA)			
Mean flow velocity, cm/s	25.1±11.0	36.4±11.6	<0.01
Diameter, mm	3.21±0.32	3.65±0.49	<0.01
TCCS findings (MCA)			
Mean flow velocity, cm/s	48.6±12.9	60.0±13.0	<0.001
SPECT findings (MCA)			
rCBF, mL/100 g per minute	37.7±6.1	41.1±5.4	<0.001
ACZ reactivity, %	5.8±9.7	21.7±15.5	<0.0001

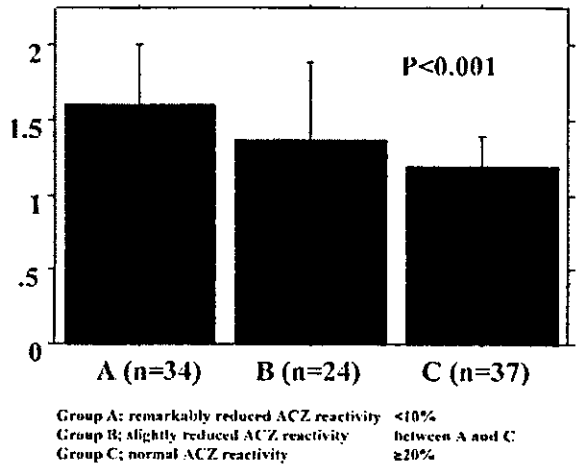

Figure 4. Grade of ACZ reactivity and changes in MCA flow velocity after CEA.

There have been many studies in which hyperperfusion syndrome was monitored using TCD.[3-6] However, because of questions regarding accuracy of TCD in diagnosing hyperperfusion syndrome, some controversy remained. Because precise placement of the sample volume as well as angle correlation is not possible by means of the TCD technique, TCD cannot determine absolute MCA flow velocity values. Tilting, rotating, or shifting of the actual location of the transducer during TCD can cause remarkable changes in flow velocity as a result of changes in the angle between the Doppler beam and the horizontal portion of the MCA. Inaccurate observation of the MCA using TCD might cause a high frequency of false-positive hyperperfusion syndrome diagnoses. For example, in the study by Dalman et al[4] with 123 subjects, TCD sensitivity for diagnosing hyperperfusion syndrome was 100%, but specificity was only 53%. In contrast, when using TCCS, one can evaluate the change in absolute value of MCA flow velocity. As well, the MFV ratio was significantly correlated with the CBF ratio. This would explain why we can predict the occurrence of hyperperfusion syndrome using TCCS with such high sensitivity and specificity.

When hyperperfusion syndrome is suspected, a strict treatment regime should be implemented immediately. Before proceeding with treatment, ability to predict hyperperfusion syndrome accurately would be desirable. In previous studies using TCD, the diagnostic criterion of hyperperfusion syndrome was mostly a ≥2-fold increase in MCA peak systolic or MFV after CEA.[3,4,6] In this study, an MFV ratio of ≥1.5 within 4 postsurgical days yielded a sensitivity of 100% and a specificity of 84%. An MFV ratio of ≥1.4 the next morning

after CEA was another indicator that predicted hyperperfusion syndrome perfectly, although its specificity was relatively low (67%). A maximum MFV ratio cut-off value of 2 within 4 postsurgical days yielded a sensitivity of 75% and a specificity of 99%. In our hospital, when an MFV ratio of ≥1.5 was observed within 4 days after CEA, the patients received more strict blood pressure control with or without a continuation of propofol sedation until the next TCCS evaluation. Propofol decreases the cerebral oxygen metabolism with a consequent CBF reduction.[17] As well, with cerebral dysautoregulation, a decrease in systemic blood pressure could result directly in a CBF decrease. This might be the reason that CBF increase in present patients after CEA was not so high compared with previous studies in which the CBF increase in the ipsilateral MCA territory was ≥100%.[18,19]

For multivariate analysis, reduction of presurgical ACZ reactivity in the affected MCA territory was an independent predictor for an MFV ratio of >1.5 within 4 postsurgical days. Several studies have also shown an association between impaired vasodilatory capacity and hyperperfusion syndrome.[18,20] Moreover, intraoperative transcranial regional cerebral oxygen saturation is another essential indicator for post-CEA hyperperfusion syndrome.[21] Ascher et al demonstrated that contralateral CEA within 3 months was associated with post-CEA hyperperfusion syndrome;[22] 1 of 6 patients with bilateral CEA had the syndrome in this study.

A study limitation is high frequency of post-CEA hyperperfusion syndrome (13%) compared with that in previous studies (1% to 3%).[2,22,23] Difference in diagnostic criteria for the syndrome might be a reason for the frequency variance between studies. Especially, consciousness deterioration and headache are frequent symptoms for post-CEA patients, which often but not always indicate hemispheric hyperperfusion. To select patients strictly with hyperperfusion syndrome, we regarded deterioration of consciousness level with remarkably abnormal speech and conduct for >6 hours after stopping sedation as presenting hyperperfusion syndrome. We did not regard patients presenting only headache as having the syndrome.

In conclusion, MFV ratio can be measured serially using TCCS with echo contrast agents, and it reflects changes in cerebral hemodynamics after CEA. Using the MFV ratio, we can accurately predict which patients are in the high-risk group for developing hyperperfusion syndrome.

Acknowledgments

This work was supported in part by research grants for cardiovascular disease (14C-1, 14A-3, 15C-1) from the Ministry of Health, Labor, and Welfare of Japan.

References

1. Sundt TM, Sandok BA, Whisnant JP. Carotid endarterectomy. Complications and preoperative assessment of risk. *Mayo Clin Proc*. 1975;50:301–306.
2. Archie JP. Carotid endarterectomy with reconstruction techniques tailored to operative findings. *J Vasc Surg*. 1993;17:141–151.
3. Schaafsma A, Veen L, Vos JP. Three cases of hyperperfusion syndrome identified by daily transcranial Doppler investigation after carotid endarterectomy. *Eur J Vasc Endovasc Surg*. 2002;23:17–22.
4. Dalman JE, Beenakkers IC, Moll FL, Leusink JA, Ackerstaff RGA. Transcranial Doppler monitoring during carotid endarterectomy helps to identify patients at risk of postoperative hyperperfusion. *Eur J Vasc Endovasc Surg*. 1999;18:222–227.
5. Powers AD, Smith RR. Hyperperfusion syndrome after carotid endarterectomy: a transcranial Doppler evaluation. *Neurosurgery*. 1990;26:56–60.
6. Keunen R, Nijmeijer HW, Tavy D, Stam K, Edelenbosch R, Muskens E, Bruijninckx C, Sier H. An observational study of pre-operative transcranial Doppler examinations to predict cerebral hyperperfusion following carotid endarterectomies. *Neurol Res*. 2001;23:593–598.
7. Bogdahn U, Becker G, Winkler J, Greiner K, Perez J, Meurers B. Transcranial color-coded real-time sonography in adults. *Stroke*. 1990;21:1680–1688.
8. Tsuchiya T, Yasaka M, Yamaguchi T, Kimura K, Omae T. Imaging of the basal cerebral arteries and measurement of blood velocity in adults by using transcranial real-time color flow Doppler sonography. *Am J Neuroradiol*. 1991;12:497–502.
9. Gahn G, Gerber J, Hallmeyer S, Reichmann H, von Kummer R. Noninvasive assessment of the circle of Willis in cerebral ischemia: the potential of CT angiography and contrast-enhanced transcranial color-coded duplexsonography. *Cerebrovasc Dis*. 1999;9:290–294.
10. Goertler M, Kross R, Baeumer M, Jost S, Grote R, Weber S, Wallesch CW. Diagnostic impact and prognostic relevance of early contrast-enhanced transcranial color-coded duplex sonography in acute stroke. *Stroke*. 1998;29:955–962.
11. Biller J, Feinberg WM, Castaldo JE, Whittemore AD, Harbaugh RE, Dempsey RJ, Caplan LR, Kresowik TF, Matchar DB, Toole JF, Easton JD, Adams HP Jr, Brass LM, Hobson RW II, Brott TG, Sternau L. Guidelines for carotid endarterectomy: a statement for healthcare professionals from a special writing group of Stroke Council, American Heart Association. *Stroke*. 1998;29:554–562.
12. North American Symptomatic Carotid Endarterectomy Trial Collaborators. Beneficial effect of carotid endarterectomy in symptomatic patients with high-grade carotid stenosis. *N Eng J Med*. 1991;325:445–453.
13. Yasaka M, Kimura K, Otsubo R, Isa K, Wada K, Nagatsuka K, Minematsu K, Yamaguchi T. Transoral carotid ultrasonography. *Stroke*. 1998;29:1383–1388.
14. Kishikawa K, Kamouchi M, Okada Y, Inoue T, Ibayashi S, Iida M. Evaluation of distal extracranial internal carotid artery by transoral carotid ultrasonography in patients with severe carotid stenosis. *Am J Neuroradiol*. 2002;23:924–928.
15. van Laere K, Van de Wiele C, Van Belle Y, Audenaert K, Dierckx R. Variability study of a non-invasive approach to the absolute quantification of cerebral blood flow with ^{99m}Tc^{m}-ECD using aortic activity as the arterial input estimate. *Nucl Med Commun*. 1999;20:33–40.
16. Matsuda H, Yagishita A, Tsuji S, Hisada K. A quantitative approach to technetium-99m ethyl cysteinate dimmer: a comparison with technetium-99m hexamethylpropylene amine oxime. *Eur J Nucl Med*. 1995;22:633–637.
17. Stephan H, Sonntag H, Schenk HD, Kohlhausen S. [Effect of Disoprivan (propofol) on the circulation and oxygen consumption of the brain and CO_2 reactivity of brain vessels in the human]. *Anaesthesist*. 1987;36:60–65. In German.
18. Hosoda K, Kawaguchi T, Shibata Y, Kamei M, Kidoguchi K, Koyama J, Fujita S, Tamaki N. Cerebral vasoreactivity and internal carotid artery flow help to identify patients at risk for hyperperfusion after carotid endarterectomy. *Stroke*. 2001;32:1567–1573.
19. Piepgras DG, Morgan MK, Sundt TM Jr, Yanagihara T, Mussman LM. Intracerebral hemorrhage after carotid endarterectomy. *J Neurosurg*. 1988;68:532–536.
20. Hosoda K, Kawaguchi T, Ishii K, Minishima S, Shibata Y, Iwakura M, Ishiguro S, Kohmura E. Prediction of hyperperfusion after carotid endarterectomy by brain SPECT analysis with semiquantitative statistical mapping method. *Stroke*. 2003;34:1187–1193.
21. Ogasawara K, Konno H, Yukawa H, Endo H, Inoue T, Ogawa A. Transcranial regional cerebral oxygen saturation monitoring during carotid endarterectomy as a predictor of postoperative hyperperfusion. *Neurosurgery*. 2003;53:309–315.
22. Ascher E, Markevich N, Schutzer RW, Kallakuri S, Jacob T, Hingorani AP. Cerebral hyperperfusion syndrome after carotid endarterectomy: predictive factors and hemodynamic changes. *J Vasc Surg*. 2003;37:769–777.
23. Coutts SB, Hill MD, Hu WY, Sutherland GR. Hyperperfusion syndrome: toward a stricter definition. *Neurosurgery*. 2003;53:1053–1060.

Journal of Cerebral Blood Flow & Metabolism
24:1359–1368 © 2004 The International Society for Cerebral Blood Flow and Metabolism
Published by Lippincott Williams & Wilkins, Baltimore

Anti–Monocyte Chemoattractant Protein-1 Gene Therapy Protects Against Focal Brain Ischemia in Hypertensive Rats

*Yasuhiro Kumai, *Hiroaki Ooboshi, *Junichi Takada, *Masahiro Kamouchi, *Takanari Kitazono, †Kensuke Egashira, *Setsuro Ibayashi, and *Mitsuo Iida

*Departments of *Medicine and Clinical Science and †Cardiovascular Medicine, Graduate School of Medical Sciences, Kyushu University, Fukuoka, Japan*

Summary: Monocyte chemoattractant protein-1 (MCP-1) is expressed in the ischemic cortex after focal brain ischemia and appears to exacerbate ischemic damage. The authors examined the effect of gene transfer of dominant negative MCP-1, called 7ND, 90 minutes after induction of focal brain ischemia in hypertensive rats. Adenoviral vectors encoding mutant MCP-1 (Ad7ND; n = 11), or *Escherichia coli* β-galactosidase (AdlacZ; n = 17) as control were injected into the lateral ventricle of male spontaneously hypertensive rats. Both AdlacZ (n = 12) and Ad7ND (n = 6) administration provided transgene expression as early as 6 hours after injection and the expression further increased on day 1, followed by a sustained detection on day 5. Five days after ischemia, infarct volume (75 ± 13 mm^3, n = 5, mean ± SD) significantly reduced to 72% of control (104 ± 22 mm^3, n = 5, $P < 0.05$) by 7ND gene transfer. Numbers of leukocytes in the vessels (48.3 ± 32.9/cm^2) and macrophage/monocyte infiltration (475.2 ± 125.5 /mm^2) of the infarct area in the Ad7ND group were significantly less than those measured in the AdlacZ group (143.8 ± 72.1/cm^2 and 671.8 ± 125.5/mm^2, $P < 0.05$, respectively). In summary, the postischemic gene transfer of dominant negative MCP-1 attenuated the infarct volume and infiltration of inflammatory cells, suggesting potential usefulness of the anti–MCP-1 gene therapy. **Key Words:** Adenovirus—Cerebral ischemia—Gene therapy—Neuroprotection—MCP-1.

Gene transfer is an attractive intervention for studies of basic mechanisms of neurobiology, and potentially for therapy of cerebrovascular disease (Heistad and Faraci, 1996; Verma and Somia, 1997). Although several studies have shown usefulness of gene transfer to the brain to protect against ischemic damage, vectors were introduced in the brain before induction of brain ischemia (Betz et al., 1995; Lawrence et al., 1996; Linnik et al., 1995; Yenari et al., 1998). To rationalize gene therapy for brain ischemia, it is important to show efficacy of gene transfer even when vectors are administered after induction of brain ischemia. We have recently shown that gene transfer can be accomplished after induction of brain ischemia either to brain parenchyma or ventricular walls (Ooboshi et al., 2001; Takada et al., 2002; Kumai et al., 2003).

Monocyte chemoattractant protein-1 (MCP-1) is a member of the C-C chemokine subfamily of chemokines (Rollins, 1996), and has chemoattractant properties for monocytes, memory T-cells, and natural killer cells (Allavena et al., 1994; Carr et al., 1994; Matsushima et al., 1989; Valente et al., 1996; Yoshimura et al., 1989). In experimental brain ischemia model, MCP-1 messenger RNA and MCP-1 protein in the ischemic cortex are expressed after focal brain ischemia (Che et al., 2001; Kim et al., 1995; Wang et al., 1995). Recent studies using genetic models have reported that MCP-1 deficiency attenuates infarct volume in the murine stroke model (Hughes et al., 2001), and overexpression of MCP-1 causes larger infarct volume and more chemoattraction of monocytes and macrophages into ischemic region than wild-type control (Chen et al., 2003), suggesting that elevated MCP-1 levels might lead to an increased influx of monocytes and evolution of size in brain infarction.

We have recently reported that an N-terminal deletion mutant of human MCP-1 gene (7ND), which lacks the N-terminal amino acids 2 to 8, acts as a dominant nega-

Received April 6, 2004; final version received June 14, 2004; accepted July 26, 2004.

This work was supported in part by a research grant in aid from the Ministry of Health and Welfare Comprehensive Research on Aging and Health (H11-008) of Japan, and from the Ministry of Education, Science and Culture (14570604) of Japan (H. O.).

Address correspondence and reprint requests to Dr. Hiroaki Ooboshi, Department of Medicine and Clinical Science, Graduate School of Medical Sciences, Kyushu University, Maidashi 3-1-1, Higashi-ku, Fukuoka 812-8582, Japan; e-mail: ooboshi@intmed2.med.kyushu-u.ac.jp

DOI: 10.1097/01.WCB.0000143534.76388.3C

tive inhibitor for MCP-1 and blocks the MCP-1/CCR2 signal pathway *in vivo* (Egashira et al., 2000; Egashira, 2003). This mutant MCP-1 and normal MCP-1 form a heterodimer, which binds to the MCP-1 receptor (CCR-2) and completely inhibits MCP-1–mediated monocyte chemotaxis *in vitro* (Rollins, 1996). In this study, we delivered the adenoviral vector encoding 7ND into the cerebral ventricle 90 minutes after focal brain ischemia, and examined whether anti–MCP-1 gene therapy would protect against focal brain ischemia.

MATERIALS AND METHODS

Adenoviral vectors

We used replication-deficient recombinant adenoviral vectors expressing *Escherichia coli* β-galactosidase (AdlacZ) or mutant MCP-1 (Ad7ND). An N-terminal deletion mutant of human MCP-1, called 7ND, lacks the amino-terminal amino acids 2 to 8. The 7ND was constructed by recombinant polymerase chain reaction using a wild-type human MCP-1 cDNA as the template and cloned into *Bam*HI (5′) and *Not*I (3′) sites of the pcDNA3 expression vector (Egashira et al., 2000, Ni et al., 2001). The DNA constructs of vectors composed of a full-length copy of the adenovirus genome of approximately 36 kb, from which the early region 1 gene (E1) was replaced by the CAG (cytomegalovirus enhancer, chicken β-actin enhancer-promoter and rabbit β-globin poly-A signal) promoter and a cDNA for lacZ or 7ND. Recombinant viruses were grown in human embryonic kidney (HEK) 293 cells that complemented the E1 early viral promoters, and were triple plaque purified to assure that viral suspensions were free of wild-type viruses. Viral titer was determined by plaque assay on HEK 293 cells. After purification, the virus was suspended in phosphate-buffered saline (PBS) with 3% sucrose, and was kept at −80°C until further use.

Animals

All animal procedures were approved by the Animal Care and Use Review Committee at the Kyushu University (12-053-0). Twenty-eight male spontaneously hypertensive rats (SHR), aged 5 to 10 months and weighing 320 to 400 g, were used. Eighteen rats were semiquantitatively or quantitatively analyzed for transgene expression of β-galactosidase or 7ND, and 10 rats were used for the brain ischemia study.

Histochemical analysis of gene expression

Twelve male SHR were quantitatively analyzed for transgene expression of β-galactosidase. Briefly, rats were anesthetized with pentobarbital (65 mg/kg, intraperitoneal injection) and mounted on a stereotaxic head holder in the prone position. A 2-cm incision was made vertically midway. Rectal and head temperature was maintained at 37°C and 36°C, respectively, by means of a warming lamp and a heating pad. For the injection of adenoviral vectors into the left ventricle, a small burr hole was made in the parietal region (1.5 mm posterior and 1.0 mm lateral to the bregma) with a dental drill. A 27-G needle on a Hamilton syringe was stereotaxically inserted into the left lateral ventricle (4.5 mm deep), and 30 μL of AdlacZ (1.3×10^9 plaque forming units per milliliter, n = 12) was injected over 10 minutes. Efficacy of transgene expression to the brain was assessed 6 hours (n = 1), 12 hours (n = 2), 1 day (n = 3), 3 days (n = 2), 5 days (n = 3), and 7 days (n = 1) after injection of AdlacZ. After the designated survival periods, the rats were killed with an intraperitoneal injection of pentobarbital and perfused transcardially with 2% paraformaldehyde and 0.2% glutaraldehyde in PBS. The brain was removed and washed thoroughly with PBS. The brain was cut into coronal sections at intervals of 2 mm and incubated in 5-bromo-4-chloro-3-indolyl-β-D-galactopyranoside (X-Gal; Wako Pure Chemical, Osaka, Japan) staining solution for 3 hours at room temperature, rinsed in PBS, and postfixed with 4% formaldehyde. Incubation with X-Gal was limited to 3 hours to prevent staining of endogenous β-galactosidase, which may be seen in the cytosol after longer periods (>4 hours) of incubation (Lal et al., 1994). Four slices that contained lateral ventricles in each rat were examined for positive staining of β-galactosidase (blue staining) in the macroscopic view. Expression of β-galactosidase in the left ventricle was analyzed semiquantitatively, and estimated with a four-point scale (0 = no stain, 1 = modest or approximately 1% to 25% area of stained blue in the ventricular wall, 2 = moderate or 26% to 75% area of stained blue in the ventricular wall, and 3 = marked or >75% area of stained blue in the ventricular wall) as described previously (Kumai et al., 2003; Ooboshi et al., 2001). The scores of four slices were averaged and used as expression score.

Measurement of 7ND

Six male SHR, weighing 370 to 400 g, were quantitatively analyzed for transgene expression of 7ND. In this experiment, procedures for operation were similar to those described for the previous experiment, except for the type of adenoviral vector. Thirty microliters of AdlacZ (1.3×10^9 plaque forming units per milliliter, n = 3) or Ad7ND (1.3×10^9 plaque forming units per milliliter, n = 3) was injected over 10 minutes. Six hours, 1 day, and 5 days after injection of vector, rats were anesthetized with pentobarbital (65 mg/kg, intraperitoneal injection) and the CSF was withdrawn (Ooboshi et al., 1995, 1997). The CSF concentration of 7ND released by transfected ependyma was measured by using sandwich enzyme-linked immunosorbent assay (ELISA) of human MCP-1. The ELISA kit (R&D Systems, Minneapolis, MN, U.S.A.) with the monoclonal antibody was used as reported previously according to the manufacturer's instructions (Kohara et al., 2002). The antibody does not cross-react with rat MCP-1.

Brain ischemia

Ten male SHR were used for the brain ischemia study. Briefly, rats were anesthetized with halothane (3% for induction; 1.5% during the surgical preparation, with a facemask; 0.75% after intubation; and 0.5% for maintenance) in a mixture of 70% nitrous oxide and 30% oxygen. The right femoral artery and vein were cannulated using PE-50 tubing. The rats were endotracheally intubated with PE-240 tubing. Pancuronium bromide (an initial dose of 0.3 mg followed by 0.1 mg every 30 minutes) was intravenously injected, and the rats were mechanically ventilated. Mean arterial pressure was continuously monitored. Physiologic variables were measured before and 1 hour after the distal middle cerebral artery (MCA) occlusion. Rectal and head temperature was maintained at 37°C and 36°C, respectively, by means of a warming lamp and a heat pad.

The rat was mounted on a stereotaxic headholder in the prone position, and a 2-cm incision was made vertically midway between the right orbit and the right external auditory canal. The temporal muscle was separated and, under an operating microscope, a burr hole 3 mm in diameter was made 1 mm posterior to the anterior junction of the zygoma and squamosal bone, revealing the distal segment of MCA above the rhinal fissure. The dura was left intact. Cerebral blood flow (CBF) before and during ischemia at the parietal cortex was measured by laser Doppler flowmetry. A burr hole, 2 mm in

diameter, was made in the parietal cortex at 4 mm lateral and 1.5 mm posterior to the bregma in the ipsilateral to ischemic side. The resting CBF value was regarded as baseline and changes after induction of brain ischemia were expressed as percentages of the resting value.

Brain ischemia was produced by photochemical occlusion of the distal MCA of SHR as described previously (Yao et al., 1996). A krypton laser operating at 568 nm (Innova 301, Coherent Inc., Santa Clara, CA, U.S.A.) was used to irradiate the distal MCA at a power of 20 mW. The laser beam was focused with a 30-cm focal length cylindrical lens (CKX 300; Newport Corporation, Irvine, CA, U.S.A.) and positioned with a mirror onto the distal MCA. The photosensitizing dye, rose bengal (15 mg/mL in 0.9% saline; Wako Pure Chemical), was administered intravenously to a body dose of 20 mg/kg over 90 seconds simultaneously with 4 minutes of laser irradiation.

For the injection of adenoviral vectors into the lateral ventricle contralateral to the ischemic side, a small burr hole was made in the parietal region as the above experiments. Ninety minutes after induction of ischemia, 30 μL of viral suspension of AdlacZ (1.3×10^9 plaque forming units per milliliter, n = 5) or Ad7ND (1.3×10^9 plaque forming units per milliliter, n = 5) was injected into the lateral ventricle over 10 minutes. Two hours after the distal MCA occlusion, the head wound was closed and the catheters were removed. The rats were carefully weaned from the respirator and returned to the home cage after regaining the ability to breathe independently. After the injection of vectors, the rats were housed for 5 days.

Quantification of brain infarction and infiltration leukocyte

Five days after brain ischemia, rats were anesthetized with pentobarbital. The brain was removed, washed thoroughly with PBS, and cut into coronal sections at intervals of 2 mm followed by postfixation with 4% formaldehyde. The fixed tissue was then processed for paraffin embedding, and sections (5 μm thick) were cut from the block with microtomes for hematoxylin-eosin staining. Morphometric determination of infarct volume by the direct method has been described previously (Liu et al., 1989). The cross-sectional area of infarct was measured with NIH Image software (version 1.63) and infarct volume of each rat was calculated.

The number of polymorphonuclear and mononuclear leukocytes in blood vessels at the infarct area was determined in the coronal slice at the level of caudate-putamen by hematoxylin-eosin staining. The number of leukocytes was divided by infarct area, and was expressed as number per square centimeter.

Immunohistochemistry of macrophage

For immunohistochemistry, paraffin slices 5 μm thick at the caudate-putamen level were preincubated with 3% skim milk to decrease nonspecific binding. Sections were incubated overnight at 4°C with the mouse anti–rat macrophage/monocyte antibody (ED1, Serotec, Oxford, U.K.) diluted 1:1000, or nonimmune mouse IgG (Santa Cruz Biotechnology Inc., Santa Cruz, CA, U.S.A.) diluted 1:1000 as negative control. The slides were washed and incubated with biotinylated, affinity-purified rabbit anti-mouse IgG (Nichirei Corporation, Tokyo, Japan) as the secondary antibody. After avidin-biotin amplification, the slides were incubated with 3′,3′-diaminobenzidine. For quantification, the number of ED1-positive cells at the ischemic area was analyzed with NIH Image software (version 1.63), and was expressed as number per square millimeter. The slides were counterstained with hematoxylin for nuclear staining.

Statistical analysis

Data are presented as means and standard deviations. Differences in physiologic variables, infarct volume, and number of leukocytes and ED1-positive cells between groups were analyzed by unpaired *t*-test. Differences in amount of 7ND were analyzed with repeated measure one-way analysis of variance followed by Bonferroni post hoc *t*-test. $P < 0.05$ was regarded as statistically significant.

RESULTS

Transgene expression of β-galactosidase

Expression of the reporter gene was consistently detected at the periventricular areas since 6 hours to 7 days after gene transfer (Fig. 1A). X-Gal staining was not

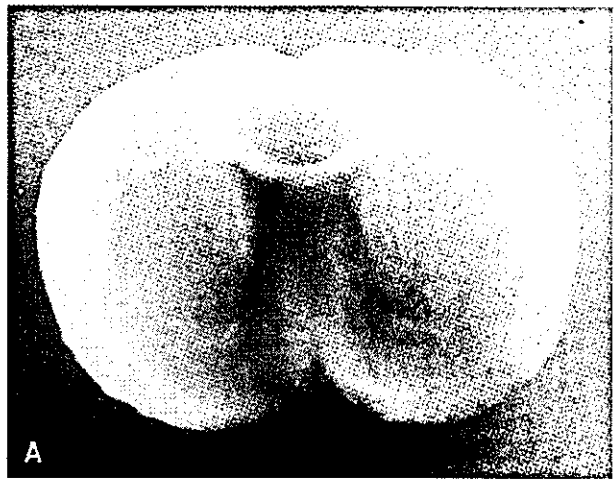

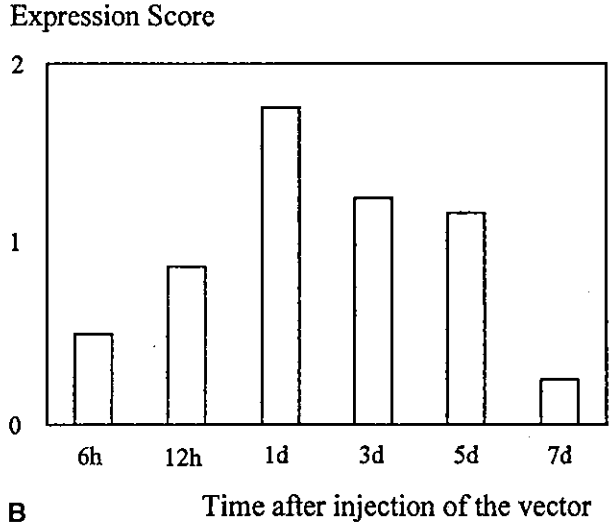

FIG. 1. Transgene expression in rat brains after gene transfer. (A) Coronal section of the brain 1 day after the ischemic insult. The transgene (β-galactosidase) was expressed at the lateral ventricles as a blue color with X-Gal staining. (B) Transgene expression was assessed at the ventricle 6 hours (n = 1), 12 hours (n = 2), 1 day (n = 3), 3 days (n = 2), 5 days (n = 3), and 7 days (n = 1) after injection of AdlacZ, and mean values are shown. The expression was observed at the ependyma as early as 6 hours after gene transfer of β-galactosidase, and peaked at day 1 followed by gradual decreases.

observed in the cortex, as reported previously (Kumai et al., 2003). The time course of semiquantitative analysis for transgene expression at the periventricular area is shown in Fig. 1B. Transgene expression was observed at the ependyma as early as 6 hours after gene transfer, and peaked at day 1 followed by gradual decreases.

Measurement of 7ND

Values of ELISA for 7ND in the CSF from the Ad7ND group are shown in Fig. 2. A marked amount of 7ND was detected 6 hours after gene transfer (8,010 ± 1,965 pg/mL). Amounts of dominant negative MCP-1 were significantly increased at day 1 and day 5 (43,600 ± 866 and 19,467 ± 5,105 pg/mL, respectively) as compared with those seen at 6 hours ($P < 0.01$). In the AdlacZ group and in normal rats, 7ND was undetectable in the CSF.

Physiologic variables

Physiologic variables before and after ischemia in AdlacZ and Ad7ND groups are shown in Table 1. There were no significant differences in physiologic variables before and after ischemia between the two groups. Blood flow to the cortex on the occlusion side began to decrease within 10 minutes after focal ischemia and lasted for more than 60 minutes. CBF reductions in AdlacZ and Ad7ND group at 60 minutes were −62% ± 17% and −69% ± 10%, respectively. Changes in CBF were not significantly different between the two groups (Fig. 3).

Infarct volume and leukocyte infiltration

Infarct volume in the AdlacZ and Ad7ND groups is shown in Fig. 4. Infarct volume in the Ad7ND group (75 ± 13 mm^3) was significantly smaller (by 28%) than that observed in the AdlacZ group (104 ± 22 mm^3, $P < 0.05$). Numbers of total and mononuclear leukocytes in the vessels at the infarct area in the Ad7ND group were 48.3 ± 32.9/cm^2 and 35.3 ± 27.7/cm^2, and were significantly smaller than those measured in the AdlacZ group (143.8 ± 72.1/cm^2 and 89.6 ± 40.9/cm^2, respectively; $P < 0.05$) (Fig. 5). Numbers of polynuclear leukocytes in the vessels at the infarct area tended to be lower in the Ad7ND group (13.0 ± 10.1/cm^2) than in the AdlacZ group (54.2 ± 13 /cm^2, $P = 0.07$).

TABLE 1. *Physiologic variables*

	AdlacZ (n = 5)	Ad7ND (n = 5)
At rest		
Body weight (g)	368 ± 22	366 ± 38
Head temperature (°C)	35.8 ± 0.2	35.8 ± 0.1
Rectal temperature (°C)	36.9 ± 0.1	37.1 ± 0.1
MABP (mm Hg)	181 ± 21	178 ± 13
Ht (%)	44.8 ± 0.8	44.0 ± 0.7
pH	7.42 ± 0.03	7.41 ± 0.04
$Paco_2$ (mm Hg)	37.2 ± 2.3	37.9 ± 3.7
Pao_2 (mm Hg)	131 ± 15	133 ± 11
BS (mg/dL)	139 ± 4	143 ± 13
One hour after dMCAO		
Head temperature (°C)	35.9 ± 0.2	35.9 ± 0.3
Rectal temperature (°C)	36.9 ± 0.2	37.1 ± 0.2
MABP (mm Hg)	203 ± 41	192 ± 19
Ht (%)	44.4 ± 0.5	43.6 ± 1.1
pH	7.40 ± 0.19	7.41 ± 0.02
$Paco_2$ (mm Hg)	36.0 ± 2.8	36.4 ± 3.2
Pao_2 (mm Hg)	133 ± 9	123 ± 8
BS (mg/dL)	122 ± 7	123 ± 10

Values are mean ± SD.
Ht, hematocrit; BS, blood sugar.

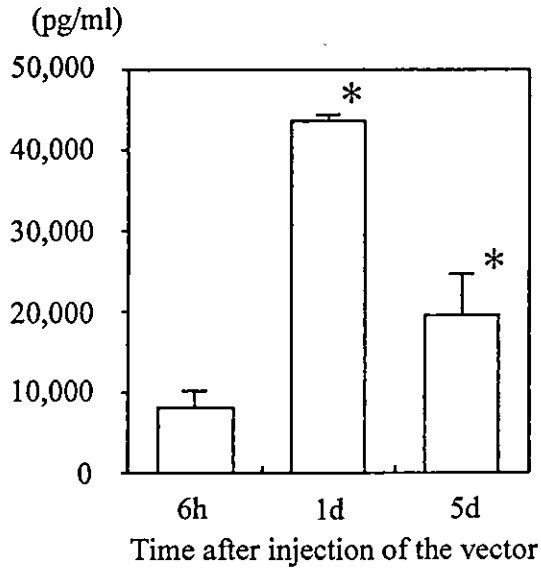

FIG. 2. Amount of dominant negative MCP-1 (7ND) in the CSF after gene transfer. A marked amount of 7ND was detected 6 hours after gene transfer. The level of 7ND at days 1 and 5 was significantly increased as compared with that at 6 hours ($P < 0.01$). Values are mean ± SD. *$P < 0.01$ versus 6 hours.

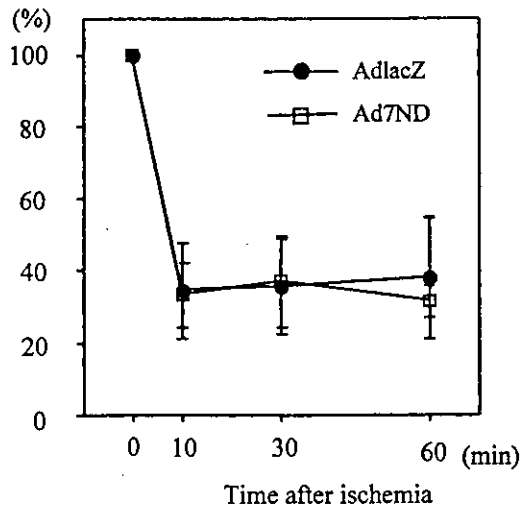

FIG. 3. Changes in cerebral blood flow at parietal cortices during distal middle cerebral artery occlusion. Blood flow to the cortex on the occlusion side began to decrease within 10 minutes after focal ischemia and lasted for more than 60 minutes. Changes in CBF were not significantly different between the two groups. Values are mean ± SD.